CHONDROITIN SULFATE MICROPARTICLES MODULATE TGF-B1-INDUCED CHONDROGENESIS IN HUMAN MESENCHYMAL STEM CELL SPHEROIDS

A Thesis
Presented to
The Academic Faculty

by

Melissa C. Goude

In Partial Fulfillment
of the Requirements for the Degree
Master of Science in the
Department of Biomedical Engineering

Georgia Institute of Technology
August 2014

CHONDROITIN SULFATE MICROPARTICLES MODULATE TGF-B1-INDUCED CHONDROGENESIS IN HUMAN MESENCHYMAL STEM CELL SPHEROIDS

Approved by:

Dr. Johnna S. Temenoff, Advisor
Department of Biomedical Engineering
Georgia Institute of Technology

Dr. Krishnendu Roy
Department of Biomedical Engineering
Georgia Institute of Technology

Dr. Todd C. McDevitt, Advisor
Department of Biomedical Engineering
Georgia Institute of Technology

Dr. Alexandra Peister
Department of Biology
Morehouse College

Date Approved:

ACKNOWLEDGEMENTS

I would like to acknowledge all of the people who have supported me and contributed to this work at Georgia Tech and Emory. Foremost, I would like to thank my advisors, Dr. Johnna Temenoff and Dr. Todd McDevitt, for the opportunity to work with them. They have given me guidance and encouragement to become a better researcher. I appreciate their willingness to listen and work with me as I completed my academic and career goals. I would also like to thank Dr. Krishnendu Roy and Dr. Alexandra Peister for agreeing to be part of my committee and for their input on my project.

I am thankful for having worked with the McDevitt Lab and the staff members in the Department of Biomedical Engineering (Sally Gerrish and Shannon Sullivan) and the Institute for Bioengineering and Biotechnology. I am particularly grateful for the members of the Temenoff Lab: Jen Lei for always being a friendly and helpful presence, Tobias Miller for his technical brilliance and honest opinion, Song Seto for her wisdom and groundedness, and Torri Rinker for being a wonderful friend with whom I faced various challenges in lab and in life. I truly felt that we were a family, supporting each other through both the good and the bad times together. I appreciated everyone's willingness to listen and provide each other support, be it technical or moral. I also want to acknowledge former Temenoff Lab members: Peter Yang and Jeremy Lim, who were both great mentors to me. Peter was willing to share with me his own experience in the program when I first joined the lab without hesitation. He was always willing to give advice in order for me to achieve a productive and positive grad school experience. I would like to especially thank Jeremy for training me when I started working on the project. He was more than patient and thorough in teaching me, allowing me to ask

endless questions and follow him around the lab. His caring and thoughtful guidance helped ease my transition into the lab.

I need to also thank Marian Hettiaratchi, Ariel Kniss, Shereka Banton and others who started in the BME program with me for their friendship and camaraderie. From surviving Mass Transfer to acing the quals, we have supported each other in achieving the milestones of grad school together. I have enjoyed exploring Atlanta together with them and sharing many great memories. I would like to especially thank Torri for having been a wonderful friend and colleague. I truly appreciated the bond we shared as we faced various challenges together in lab and in life.

Most importantly, I would like to acknowledge my family, who has been my biggest supporters. I have been fortunate to have such close bonds with my family. My parents have always given me love and support in their own ways, wanting nothing but the best opportunities for me as I encounter each stage of my life. My Dad has taught me to work hard and he has never doubted my ability to excel. Through all of the challenges that I have had to face, my Mom has been a pillar of strength for me, guiding me with her selflessness and wisdom. Even in times of desperation, she has never failed to maintain an optimistic and confident outlook. I have nothing but the utmost respect for her; she is my role model. My younger brother, Eddie Goude, has also been a joyful encouragement. He has never failed to bring out the silliness and laughter in me when I felt down. I am so proud to see him graduate from college, mature and finally get ahead of his sister by making his foray into the corporate world as a software engineer. I thank my family for their unconditional love; I would not have all of my accomplishments without their support.

TABLE OF CONTENTS

LIST OF TABLES

LIST OF FIGURES

LIST OF ABBREVIATIONS

ADAMTS	a disintegrin and metalloproteinase with thrombospondin motifs
α-MEM	Minimum Essential Medium-alpha
ANOVA	analysis of variance
α –SMA	α-smooth muscle actin
BM	bone marrow
BMP	bone morphogenetic protein
cMSC	caprine MSC
CS	chondroitin sulfate
CSMA	chondroitin sulfate methacrylate
CS-NHS	chondroitin sulfate-n-hydroxysuccinimide
DMEM	Dulbecco's Modified Eagle Medium
ECM	extracellular matrix
EDC	N-(3-dimethylamino propyl)-N'-ethyl carbodiimide hydrochloride
GAG	glycosaminoglycan
GalNAc	N-acetyl-galactosamine
H&E	hematoxylin and eosin
HA	hyaluronan
hMSC	human MSC
HIF-1α	hypoxia-inducible factor 1α
Ig	immunoglobulin
IHC	immunohistochemistry
ITS+	insulin, human transferrin, and selenous acid
μCT	micro-computed tomography

MMP	matrix metalloproteinase
MP	microparticle
MSC	mesenchymal stem cell
NCAM1	neural cell adhesion molecules 1
OCT	optimal cutting temperature compound
OPF	oligo(poly(ethylene glycol) fumarate)
PBS	phosphate buffered saline
PEG	poly(ethylene glycol)
PEG-DA	poly(ethylene glycol)-diacrylate
PEG-DMA	poly(ethylene glycol)-dimethacrylate
PLGA	poly(lactic co-glycolic acid)
PS	poly(styrene)
RT-PCR	reverse transcription polymerase chain reaction
RUNX2	runt-related transcription factor 2
SOX9	(sex determining region Y)-box 9
TGF-β	transforming growth factor-β
TNFα	tumor necrosis factor α

SUMMARY

Due to the limited intrinsic healing ability of mature cartilage tissue, stem cell therapies offer the potential to restore cartilage lost due to trauma or arthritis. Mesenchymal stem cells (MSCs) are a promising cell source due to their ability to differentiate into various adult tissues under specific biochemical and physical cues. Current MSC chondrogenic differentiation strategies employ large pellets, however, we have previously developed a high-throughput technique to form small MSC aggregates (500-1,000 cells) that may reduce diffusion barriers while maintaining a multicellular structure that is analogous to cartilaginous condensations. The objective of this study was to examine the effects on chondrogenesis of incorporating chondroitin sulfate methacrylate (CSMA) microparticles (MPs) within these small MSC spheroids when cultured in the presence of transforming growth factor-β1 (TGF-β1) over 21 days. Spheroids +MP induced earlier increases in collagen II and aggrecan gene expression (chondrogenic markers) than spheroids -MP, although no large differences in immunostaining for these matrix molecules were observed by day 21. Collagen I and X was also detected in the ECM of all spheroids by immunostaining. Interestingly, histology revealed that CSMA MPs clustered together near the center of the MSC spheroids and induced circumferential alignment of cells and ECM around the material core. Because chondrogenesis was not hindered by the presence of CSMA MPs, this study demonstrates the utility of this culture system to further examine the effects of matrix molecules on MSC phenotype, as well as potentially direct differentiation in a more spatially controlled manner that better mimics the architecture of specific target tissues.

CHAPTER 1

INTRODUCTION

Background

Cartilage

Cartilage Disease

In 2005, approximately 27 million adults in the U.S. exhibited clinical osteoarthritis (OA) symptoms [1]. It has also been predicted that 1 in 2 Americans will be affected by OA in at least one knee during their lifetime [2]. Osteoarthritis is a disease that is characterized by the degeneration of articular cartilage. Often, physical trauma changes the distribution of load across the articulating surface of the joint, which leads to an abnormal tissue remodeling response [3, 4]. Irregularities on the cartilage surface first develop due to the altered joint mechanics and stability [3]. However, there is little intrinsic repair capacity in cartilage due to variety of reasons, including a lack of progenitor cell source and low proliferative and healing ability of resident chondrocytes [5]. In response to the altered mechanical force in the joint, chondrocytes that are normally in a resting state become proliferative and increase production of matrix-degrading enzymes, such as metalloproteinases [6], aggrecanses [7], and cathepsins [8]. Inflammation can also occur during the early onset of OA due to the initial trauma, in which mononuclear cells infiltrate and secrete inflammatory cytokines like interleukin 1β and tumor necrosis factor α that drive the catabolic activities in the joint by inducing more inflammatory factors (inducible nitric oxide synthase, oncostatin M …etc). [7, 9]. The fibrillar network of aggrecan is first degraded by a disintegrin and metalloproteinase

with thrombospondin motifs (ADAMTS) followed by cleavage of the collagen II by matrix metalloproteinase-13 (MMP-13) and other proteases [3, 4, 8]. The loss of the extracellular matrix (ECM) network results in large lesions in the tissue accompanied by increased swelling of the cartilage and thickening of the subchondral bone [4], which leads to decreased mechanical loading and gliding capacity that are evident in the limited joint mobility and increased pain in the patient [10].

Cartilage Composition

Hyaline cartilage is a connective tissue that lines the surface of synovial joints such as the knee, allowing articulating motion. It is a largely avascular and aneural tissue with low oxygen tension [11, 12]. The resident cell type in the cartilage is chondrocytes, which possess a mature rounded phenotype with a lack of proliferative activity [11] and are embedded within a highly organized ECM of collagen, proteoglycans, and noncollagenous molecules [13]. The macrofibrillar framework is composed mainly of collagen type II, which contributes to the stiffness of the tissue [14], with little collagen I and X [15]. Proteoglycans form a sub-lattice structure that fills the interfibrillar space and connects to the collagen fibrils, conferring high compressive properties of cartilage [12]. Articular cartilage consists of 70-80% water due to the large amounts of proteoglycans and 50-90% collagen by dry weight [11]. Comparatively, chondrocytes constitute only a small portion of the total tissue volume at 2-5% [12, 15], making cartilage an ECM-rich tissue.

Proteoglycans are composed of glycosaminoglycan (GAG) branches that are covalently attached to a core protein. Several classes of proteoglycan are found in the cartilage (aggrecan, decorin, biglycan, perlecan and fibromodulin) that differ in the

number and type of GAG branches, such as chondroitin sulfate (CS), dermatan sulfate, and keratan sulfate [16]. The GAGs enable the proteoglycan to promote collagen fibril formation [17] and regulate cell function via interactions with proteins and growth factors [18]. In particular, CS is the main GAG constituent of aggrecan, the most abundant proteoglycan in the articular cartilage [11, 12]. It is composed of repeating disaccharide units glucuronic acid and N-acetyl-galactosamine (GalNAc) with sulfation on carbon 6 of GalNAc being the most common in mature cartilage [19]. The highly sulfated CS chains impart a high anionic charge to aggrecan, allowing it to interact with ions to facilitate the diffusion of water into the cartilage [15], which is the basis for the high compressive strength of cartilage [11, 12]. The swelling of the tissue is counteracted by the tension from the collagenous network, resulting in the maintenance of osmostic pressure within the cartilage during normal mechanical loading of the joint [11, 15].

Cartilage Development

The development of cartilage for limb skeletogenesis begins in the embryo as mesenchymal cells are recruited from the lateral plate medosderm and aggregate to form a skeletal blastema [20]. Within the limb field, chondrogenically-committed mesenchymal cells condense due to cell-cell and cell-matrix interactions promoted by the expression of cell adhesion molecules (N-cadherin and neural cell adhesion molecules 1 (NCAM1)) and ECM protein (fibronectin) [21-23]. The activation of several signaling pathways also occurs during cartilaginous condensation. Wnt-mediated expression of fibroblast growth factor (FGF) and Sonic hedgehog are essential during early limb patterning for the regulation of cell proliferation within the condensation [24]. Bone morphogenetic protein (BMP) signaling is also required for the formation of cartilaginous

condensation and the subsequent differentiation of mesenchymal progenitor cells into chondrocytes [25] by regulating expression of master transcription factor (Sex Determining Region Y)-Box 9 (SOX9) early in the condensation process to for the deposition of collagen II and aggrecan later during chondrogenesis [24, 26, 27]. In forming articular cartilage, the chondroprogenitor cells differentiate into resting cells and produce aggregan-rich ECM by signaling via integrins (α1, α10, β1) and collagen receptor discoidin domain-containing receptor 2 [26]. Differentiation into chondrocytes is followed by proliferation, terminal differentiation, hypertrophy and apoptosis in order to form bone by the process of endochondral ossification [28].

Although many mechanisms still need to be elucidated, proteoglycans are essential in regulating chondrogenesis during embryonic development. Aggrecan has been shown to facilitate collagen fibrillogenesis and maintain the collagenous network during the development of cartilaginous tissues [29]. The retention of pericellular matrix also depends on the interaction of aggrecan-hyaluronan (HA) aggregates with the CD44 receptors expressed on chondrocyte surface [17]. The loss of aggrecan from the developing growth plate has been shown to result in impaired Indian hedgehog homolog, FGF, BMP signaling during chondrogenesis [30]. Together, these evidence suggests that aggrecan plays an important role in the presentation and regulation of growth factors to the maturing mesenchymal cells. Versican, another large CS proteoglycan, is highly synthesized by mesenchymal cells in the limb bud to facilitate the cellular condensation process by interacting with ECM molecules, fibronectin and collagen I [31], as well as growth factors such as transforming growth factor-β 1 (TGF-β1) [32]. Modulation of CS proteoglycan expression (i.e. decreased versican and increased aggrecan expression with

chondrocyte differentiation) helps maintain the mature chondrogenic phenotype [30]. Overall, CS proteoglycans are essential in mediating the process of chondrocyte differentiation in the cellular condensations during development.

In Vitro Chondrogenic Differentiation

Due to the inefficiency of current therapies to produce load bearing, hyaline-like cartilage [5, 13], tissue engineering strategies have been applied to improve the cartilage regeneration process. The use of chondrocytes in scaffolds for regenerating cartilage has been investigated previously [33-36]. However, the low number of chondrocytes available for harvest and associated risk for autologous donor site morbidity are serious challenges to their widespread clinical use [37]. In addition, the expansion of chondrocytes *in vitro* prior to scaffold seeding and implantation results in de-differentiation characterized by changes in gene expression (collagen I, II, and aggrecan) as early as the first passage [38]. As a result, chondrocyte-based constructs often produce low amounts of collagen, leading to reduced tensile properties relative to healthy cartilage [13] and a ratio of chondrocytes, GAG and collagen content that does not resemble that of mature cartilage.

An alternative source of cells is MSCs, which are multipotent with the capacity to differentiate into various adult tissues including cartilage under specific physical and biochemical stimuli. Chondrogenic differentiation of MSCs from a variety of tissue sources, such as adipose tissue and umbilical cord, has been attempted, but bone marrow-derived MSCs have been shown to exhibit higher chondrogenic potential [39, 40] and was chosen for this study. In order to direct chondrogenesis, material selection for the scaffold is also important due to the effects of its physical (i.e. porosity, topography,

microstructure...etc) and mechanical properties on stem cell fate [37, 41-43] and will be discussed in later sections in more details. Soluble biochemical cues have also been identified to promote chondrogenic differentiation of MSCs with TGF-β1, 2, 3 being the most common and effective in promoting GAG production and collagen II gene expression [44, 45]. Other growth factors, such as BMe-2 and 6 or insulin-like growth factor-1, further enhance the effects of TGF-β [46, 47]. The addition of dexamethasone with TGF-β also induced more homogeneous deposition of collagen II in MSCs [45, 48]. Additionally, scaffold-free high density pellet culture has been widely used to simulate the N-cadherin and NCAM1-mediated cell-cell interaction present in cartilaginous condensations [22, 24, 49-51]. However, challenges arise with the use of MSCs due to the complexity of chondrogenesis in regards to the synchronization of signaling cascades and regulatory networks, the crosstalk between genes and effector molecules, and the precise pattern of spatial and temporal control that are difficult to mimic *in vitro* [10, 24, 27]. In addition, MSCs are found to undergo terminal differentiation similar to chondrocytes during endochondral ossification, producing collagen type I and and X, alkaline phosphatase, other hypertrophic markers as well as mineralizations in many cases [52-54]. Due to the challenge in inducing and maintaining long-term chondrogenic phenotype in MSCs, modifications to standard culture conditions are being explored.

Hypoxic Culture

In attempt to reduce MSC hypertrophy found in standard differentiation conditions, low oxygen tension ranging from 1 to 5% O_2 [55-58] have been recapitulated *in vitro* as the cartilaginous condensations present during embryonic limb development has been shown to be avascular [59, 60]. Hypoxia has also been shown to prevent

chondrocyte proliferation while promoting matrix accumulation [61], by mediating the expression of transcription factor hypoxia-inducible factor 1α (HIF-1α), which can decrease osteogenic runt-related transcription factor 2 (RUNX2) gene expression and its DNA binding activity in human MSCs [55] as well as other cell types including human osteoblast-like cells [62] and mouse mesenchymal cells [63]. Additionally, HIF-1α has the ability to directly bind to the SOX9 promoter under hypoxia, thus increasing chondrogenic gene expression (collagen II and aggrecan) in MSCs and limb bud mesenchymal cells [55, 64-67].

Hypoxic culture has been shown to both reduce and delay hypertrophic collagen X expression while promoting chondrogenic gene markers in MSCs [55, 57, 58]. Sheehy et al. reported increased collagen II production with lowered collagen type X, Alizarin Red staining and alkaline phosphatase activity in porcine MSC pellets cultured under 5% O_2 [58]. Human MSCs encapsulated in alginate beads and cultured under 5% O_2 without the addition of growth factors (i.e. TGF-β) also demonstrated higher increase in collagen II and aggrecan, SOX5, 6 and 9 mRNA expression and reduced collagen X, alkaline phosphatase and RUNX2 gene expression [55]. In another study, hMSC pellets in 5% O_2 hypoxia were stimulated with either chondrogenic (TGF-β2) or hypertrophic (β-glycerophophate) medium [57]. Although collagen X protein production was detected in all pellets, the progression of hypertrophy appeared to be delayed in low oxygen tension as evidenced by the increased gene expression of late hypertrophic markers (osteopontin and osteocalcin) under normoxic conditions [57].

Despite the ability of some hypoxic culture to suppress hypertrophic expression in encapsulated MSCs or pellets [55, 57, 58], others have still reported increase in collagen

X levels [68, 69]. In one study, micropellets of hMSCs were cultured under 2% O_2 for chondrogenesis with traditional pellets as controls [70]. Increases in aggrecan and collagen II gene expression detected in hypoxic micropellets were even higher than that in hypoxic pellets, suggesting that aggregate size may play a role in hypoxia-mediated chondrogenesis. Although higher and more uniform GAG and collagen II staining was also detected in hypoxic micropellets, collagen I and X mRNA expression was markedly increased along with osteocalcin [70]. Similarly, ovine MSCs expanded under low oxygen tension (5% O_2) prior to forming pellets demonstrated increased collagen II and aggrecan gene and protein expression along with enhanced GAG deposition [68]. However, higher collagen X gene expression was still detected at day 7 in the pellets under hypoxia.

Although the review here focused primarily on bone marrow-derived mesenchymal stem cells, the cell type, species and tissue source may affect the extent of hypoxia in reducing hypertrophy [67, 69] as well as differences in the range (% O2) and duration of hypoxia. Even the maintenance of low oxygen tension during media changes [57] may be critical in preserving the effectiveness of hypoxic culture. Although hypertrophic markers may still be expressed under some hypoxic culture, the beneficial effect of hypoxia on increasing chondrogenic gene expression in MSCs has been consistently reported.

Three Dimensional Spheroid Culture

Culturing cells in a spheroid format has been used to better recapitulate the cell-cell contact and native structure of both mature and developing tissue [48, 71, 72]. Although cells are typically expanded in monolayer, two dimensional culture often leads

to decreased tissue-specific or therapeutic properties [73, 74] due to the ability of substrate to stimulate cellular differentiation via its physical or mechanical properties [42]. As a result, scaffold-free three dimensional culture has been widely explored in order to circumvent these issues. Specifically, spheroid culture is distinguished from larger aggregates or pellets in that they are typically 100 to 500μm in size, thus reducing the diffusional limitations and necrotic core that may accompany pellets greater than 500μm [73].

Spheroids have been formed with a variety of cell types, such as cancer cells [75-77], hepatocytes [78, 79], and stem cells [71, 79, 80] to study cellular behavior in tumor models, hepatic systems, high throughput drug screening, and tissue engineering strategies [73]. Spheroids can be formed by creating an environment that favor cell-cell contact, such as the use of non-adhesive or positively charged substrates to decreases cell-surface contact [75, 78, 81]. External forces can also be applied to aggregate cells, such as in hanging drop culture that forms spheroids under microgravitational at the liquid-air interface [79] or the application of external magnetic fields [77, 82] and ultrasound [76], which are less common. To scale-up the formation of spheroids, dynamic culture in spinner flasks [75] or orbital rotary systems [71, 81] have been explored. Similarly, patterns of microfabricated structures, such as microwells, using non-adhesive materials have been used to increase the throughput of aggregate formation with applied fluid flow or low-speed centrifugation to deposit cell suspension into each micro-cavity [83-88]. In addition, this technique confers the advantage of control over size and uniformity [73, 88, 89] and easily allows homogeneous incorporation of microparticles within the spheroid [80, 90].

Scaffold-free spheroid culture of MSCs is of particular interests due to the reported loss of self-renewal capability and differentiation potential in monolayer culture [74]. Not only so, the lack of similarity between a two dimensional substrate and the native stem cell niche has resulted in limited ability to improve differentiation efficiency *in vitro* [91]. Subsequently, the capability of MSC spheroids to maintain multipotency and improve differentiation has been investigated. In one study, MSCs retrieved from spheroids (300, 600, or 1,000 cells) and plated on a two dimensional substrate under differentiation cues demonstrated increased adipogenic and osteogenic differentiation potential than monolayer-expanded MSCs [80]. Furthermore, attempts to adipogenically or osteogenically differentiate MSCs in the three dimensional culture format has shown comparable increases in ECM markers [80] or higher gene and ECM expression in spheroids to MSCs in monolayer [74, 91]. Chondrogenic differentiation of MSC spheroids (~200μm) displayed increased SOX9, collagen II, and aggrecan gene expression compared to large pellets (>500μm) [70]. Not only was increased GAG and chondrogenic ECM protein deposition evident in the spheroids, but more homogenous expression was observed, suggesting that diffusional limitations in large multicellular aggregates may result in spatial heterogeneity in chondrogenesis [70]. Similar culture conditions with chondrocyte spheroids also promoted re-differentiation with increases in GAG production and collagen II gene expression [92]. Together, these evidence indicate that the three dimensional nature and small size of MSC spheroids may be more amenable for promoting cellular differentiation than monolayer or large aggregate culture.

In addition to enhancing differentiation capacity, MSC spheroid culture has exhibited other benefits, such as improved therapeutic properties. For instance, injection of MSC spheroids into a rat acute myocardial infarction model resulted in significantly higher left ventricular function after 12 weeks compared to treatment with dissociated MSCs [93]. Besides the maintenance of strong viability and lack of necrotic core [74, 80], MSC spheroids has been shown to secrete a variety of therapeutic cytokines [74, 94, 95]. Frith et al. has reported decreased viability of four different cancer cell lines after culture in media conditioned by MSC spheroids, which secreted increased amounts of tumor-suppressing interleukin-24 [74]. MSC spheroids also produced higher amounts of anti-inflammatory proteins (tumor necrosis factor α (TNFα) stimulated gene/protein 6 and staniocalcin-1) and anti-cancer proteins (interleukin-24, TNFα-related apoptosis inducing ligand and CD82) compared to monolayer MSCs, which led to increased suppression of inflammatory response *in vitro* and *in vivo* in a mouse peritonitis model [94]. Another anti-inflammatory molecule, prostaglandin E2, has also been identified in MSC spheroid-conditioned medium as a contributor to reduced macrophage proinflammatory activity [95]. The secretome profile of MSC spheroids further demonstrates the therapeutic potential of MSC beyond enhancing differentiation potential.

GAG-based Hydrogels for Cartilage Tissue Engineering

While a variety of polymers have been used to form hydrogel scaffolds for cartilage regeneration [37], GAGs is a particularly promising class of biopolymer due to their ability to interact with growth factors and attract water [18]. Because GAGs are abundant in native cartilage [12], GAG-based scaffolds may hold the potential to better

mimic the tissue structure and function. The hydrogels as discussed here are crosslinked, hydrophilic, polymeric constructs that have a high affinity for water [96] and have not undergone specific processing to create macropores or extensive interconnected porous structures. Due to the wide range of GAG-based hydrogels, examples are organized by each major GAG species, starting with the most heavily sulfated.

Heparin

Because of the high degree of sulfation along the GAG backbone, heparin-based scaffolds are often used in tissue engineering to sequester growth factors although heparin is only present in a few tissues natively [97]. In hydrogel scaffolds, heparin has often been combined with another polymer, such as linear or branched poly(ethylene glycol) (PEG) to improve handlability or tune protein release properties [98, 99]. For crosslinking, heparin has been functionalized with moieties such as thiols, maleimide and tyramine to react with PEG [14, 99, 100]. Due to the versatility of these crosslinking schemes, heparin can be used as a part of strategies to regenerate target tissues with very different biochemical and mechanical properties [101].

Heparin-PEG systems have been utilized for engineering tissues that require higher elastic moduli, such as in cartilage (tissue modulus ~1,000kPa) [14]. However, the moduli of the heparin-PEG hydrogels discussed here are still significantly lower than that of the native tissue and thus, they are may be not useful for load bearing applications without additional mechanical support. For repair of connective tissues, bovine chondrocytes have been delivered for cartilage repair in dextran-heparin hydrogels. In these studies, the increase in dextran content resulted in scaffolds of higher storage modulus up to a maximum of 48kPa [14]. However, scaffolds containing 25:75 weight

ratio of dextran and heparin demonstrated less susceptibility to hydrolytic degradation due to the stability of the urethane bond against hydrolysis [102] and enhanced collagen II and aggrecan gene expression and collagen production in chondrocytes compared to 50:50 or 75:25 dextran-heparin scaffolds [14].

Overall, the ease in functionalizing heparin for crosslinking, as well as its high level of negative charge, has promoted its use in many tissue-engineering constructs as carriers for both cells and growth factors or other proteins. In recent studies, heparin-based hydrogels have also been explored to enhance cell-derived (autocrine) signals or paracrine signaling between two cell types in order to improve differentiation of encapsulated progenitor cells. Thus, the electrostatic interactions between heparin and proteins can be employed in several paradigms in tissue engineering scaffolds as a part of regenerative approaches to a wide range of tissues.

Chondroitin Sulfate

Chondroitin sulfate is the major GAG component of cartilage ECM [16] and has the ability to bind to positively-charged proteins due to the sulfate groups along the backbone. However, CS hydrogels are not often used as stand-alone drug delivery depots, but are utilized to enhance the biochemical properties in the presence of growth factors, such as TGF-β, in cell culture media [103, 104]. CS is commonly paired with poly(ethylene glycol) (PEG) in constructs [103, 104]. To form hydrogels, CS is usually methacrylated for chemically crosslinking via free radical polymerization with either thermal [103, 105] or UV-light initiation [104, 106] in addition to crosslinking with carbodiimide chemistry [107, 108].

CS-based scaffolds have been designed to either: 1) induce chondrogenic differentiation of stem cells such as MSCs or 2) promote survival and function of differentiated chondrocytes while enhancing the tensile and compressive properties of the construct. CS in combination with various PEG crosslinkers has been used to seed human MSCs (hMSCs) [103, 104]. One study examined the effects of desulfated CS on TGF-β sequestration from the media and hMSCs chondrogenic differentiation. The results showed that aggrecan and collagen II gene expression increased in the desulfated scaffolds compared to those containing natively-sulfated CS [103]. However, little degradation in the scaffold occurred, possibly preventing ECM deposition [103]. In contrast, in another study, a cell-laden CS methacrylate-PEG-diacrylate (PEG-DA) scaffold experienced degradation due to cell-secreted enzymes that allowed caprine MSCs (cMSCs) to form cartilaginous aggregates after 3 weeks with enhanced GAG and collagen production compared to a PEG-DA only scaffold [104]. The addition of CS increased the swelling ratio and the equilibrium water content of the hydrogels relative to PEG-dimethacrylate (PEG-DMA) scaffolds. To increase control over degradation, a MMP-sensitive sequence was added to a CS-PEG-DMA hydrogel, which resulted in a scaffold that mimicked the superficial zone of cartilage. The CS-PEG-MMP peptide hydrogel promoted high collagen II synthesis in the encapsulated cMSCs and low GAGs production level after 6 weeks [106].

CS-based hydrogels have also been utilized to promote function of differentiated cells, such as chondrocytes, for cartilage tissue engineering. In order to increase swelling ratio while maintaining high modulus in the hydrogel scaffold, CS methacrylate was photocrosslinked with PEG-DMA and used to encapsulate bovine articular chondrocytes

[109]. Compared to a PEG-DMA scaffold of similar swelling ratio, the incorporation of 40% CS increased the compressive modulus of copolymer construct by 4 fold [109]. After 14-day culture, the bovine chondrocytes in CS-PEG hydrogels exhibited higher collagen II gene expression than pure CS constructs [109]. A decrease in GAG content was observed at week 4 in CS-PEG hydrogels compared to PEG-DMA controls, which may indicate possible degradation by cell-secreted enzymes [109].

Other CS-based hydrogel scaffolds function not only as an artificial ECM to promote cellular activity, but as a tissue adhesive that can be loaded with bone marrow aspirates and BMP-2 for orthopedic tissue repair [108, 110]. The articular cartilage tissue adhesive was first formulated with methacrylated CS and PEG-DA, which could be photocrosslinked *in situ* and has the capability to bond other biomaterials containing vinyl groups [111]. CS was conjugated to n-hydroxysuccinimide (CS-NHS) to react with PEG-amine through the carboxyl group or with the primary amines found in the proteins of the tissue [108]. The multifunctional CS-PEG hydrogel can be polymerized *in situ* and is degradable enzymatically by chondroitinase ABC [112], which may better promote *in vivo* tissue integration. Similarly, CS-NHS was reacted with the amines in the proteins of bone marrow (BM) aspirate to encapsulate bovine meniscal fibrochondrocytes [110]. *In vitro*, the CS-BM adhesive has been shown to promote total collagen production in encapsulated bovine chondrocytes and collagen I production in meniscus fibrochondrocytes.

CS has mainly been studied as a means to enhance the function of cells in the presence of exogenous cues as well as improve the stiffness of hydrogels without sacrificing the high water content needed for cell encapsulation. Thus, much like its

native function in cartilage, CS has been employed for both biochemical and structural reasons towards regeneration of the tissue.

Hyaluronan

Unlike other GAGs, HA is nonsulfated and therefore its major biological activity is conferred through binding to specific cell surface receptors, rather than interactions with growth factors [113]. HA is a component of every connective tissue and possesses extremely high water binding capacity [113], which makes it a strong candidate for engineering cartilaginous tissues [114]. Similar to CS, HA is often incorporated in hydrogel scaffolds to achieve both high swelling ratios and compressive moduli [115-117]. HA is often methacrylated to allow for covalent crosslinking into hydrogels [118, 119].

HA has been incorporated for engineering of orthopedic tissues. Chondrogenic differentiation of caprine MSCs (cMSCs) has been investigated in PEG-HA scaffolds over 6 weeks [120]. The presence of HA suppressed GAG deposition in the cMSCs and induced lower levels of SOX9, aggrecan, and collagen II gene expression than PEG-DA controls and PEG-collagen scaffolds, which indicated a lack of chondrogenic phenotype [120]. However, the cMSCs in the PEG-HA hydrogel stained strongly for Alizain Red and promoted the highest calcium accumulation compared to the PEG-DA and PEG-collagen hydrogels [120]. Degradation of the PEG-HA scaffold was not specifically discussed in the study [120].

Like CS, HA-based hydrogel constructs have been employed due to both their high swelling capacity as well as the potential for bioactivity of HA degradation products through interaction with specific cell surface receptors. However, because HA is natively

found in many tissues, the range of applications for which HA hydrogels have been explored is greater than CS. Like the other GAGs discussed in this section, the ability to tune levels of HA modification during synthesis allows the fabrication of crosslinked constructs with a range of mechanical properties and degradation times that can be tailored for particular regenerative medicine applications.

Injectable Cartilage Tissue-Engineered Scaffolds

Many tissue-engineered hydrogels, such as the GAG-based systems detailed in the previous sections, are applicable to an injectable delivery, which offers several advantages over pre-formed scaffolds. An injectable approach to cartilage tissue engineering is attractive due to the ability of the delivered scaffold to fill to the irregular shape of cartilage defects and its amenability towards minimally invasive arthroscopic procedure [121, 122]. To confer injectability, the viscosity of the polymer solution should allow for conformation to defect morphology and retention at the injection site prior to *in situ* crosslinking with minimal release of cytotoxic by-product [122-124]. As a result, the hydrogel scaffold is usually characterized in terms of gelation time and how the crosslinking mechanism impacts the mechanical properties and degradability of the scaffold. Naturally-derived polymers, such as alginate, fibrin, and chitosan, have been studied due to their inherent biocompatibility and biodegradability [123]. However, to improve mechanical properties and handability of hydrogel scaffolds, combinations of natural and synthetic polymers have also been developed.

Alginate was one of the first biopolymers to be used as injectable scaffold for chondrocytes and it has been shown to promote GAG production after 12 week implantation in mice [33, 36]. More recently, an alginate system that can be rapidly

crosslinked under 1 min with a Young's modulus of 0.17MPa promoted GAG and collagen II production in the encapsulated chondrocytes after 6 weeks of *in vitro* culture [125]. Despite the ease of crosslinking, the degradability of alginate has not been shown *in vivo*, which is not favorable for tissue integration during the cartilage regeneration process [126]. Conversely, a degradable fibrin mesh, which can be formed from autologous fibrinongen and thrombin, has been used as injectable glue for various tissues [126, 127] that gelates between 1 to 10 minutes [128]. After crosslinking, fibrin gels has a dynamic compressive modulus up to 4-5kPa [129] and an equilibrium modulus of ~12kPa [130], which are much lower than the mechanical properties of native cartilage. Fibrin gel has been shown to promote collagen II and SOX9 gene expression as well as GAG production in chondrocytes [129, 130]. Although *in vivo* study has demonstrated that the implanted fibrin gel can enhance GAG and collagen II production after 6 weeks [127], the low mechanical property and high degradability of fibrin scaffolds may not be ideal for engineering cartilage tissue [131].

Other naturally-derived polymers, such as chitosan, can be modified to allow for *in situ* crosslinkning with different schemes to form injectable hydrogels. A mixture of methacrylated chitosan-glycol and HA was photocrosslinked under 40 seconds, resulting in a scaffold of ~17kPa compressive modulus that underwent little hydrolytic degradation but high enzymatic degradation (~20 wt% remaining) after 42 days [132]. Alternatively, an N-succinyl-chitosan and aldehyde HA hydrogel was crosslinked under 4 min without additional chemical crosslinker based on a Schiff base reaction between the amino and aldehyde groups, achieving compressive modulus up to 28kPa with slower hydrolytic degradation as the amount of chitosan increased [133]. These chitosan-HA systems

demonstrated more safranin-o and alcian blue staining after 21 days than chitosan-only controls [132] and maintained viability of encapsulated chondrocytes [133]. Enzymatic crosslinking using horseradish peroxidase and hydrogen peroxide is an alternative method to produce injectable hydrogels composed of tyramine-conjugated heparin and dextran with encapsulated chondrocytes [14]. The gelation time was as low as 30 sec and the resulting scaffold possessed a storage moduli of 48kPa and increased CS and collagen production [14]. In a similar dextran-tyramine system without heparin, the hydrogel polymerized within 5 to 9 min with little hydrolytic degradation (less than 25 wt% loss) in 5 months [102].

Synthetic polymers, such as oligo(poly(ethylene glycol) fumarate) (OPF) and PEG, can be combined with biopolymers or used alone for injectable hydrogels. An OPF scaffold containing TGF-β1-loaded gelatin microparticles formed with a PEG-DA crosslinker under radical polymerization exhibited an elastic modulus of 20kPa [134] was able to maintain the chondrocytic phenotype for 21 days [135] and increase collagen II gene expression in MSCs after 14 days [136]. In another hydrogel system, PEG-vinylsulfone and HA-thiol were crosslinked via Michael-type addition under 1 min with a storage modulus of 1kPa showed tunable enzymatic degradation rate between 3 to 15 days and the encapsulated chondrocytes deposited GAG and collagen II after 3 weeks [137]. These hybrid injectable hydrogels employ the inherent properties of the naturally-derived polymer to enhance aspects of the system: the use of gelatin to electrostatically load TGF-β [135] and HA to increase swelling of the hydrogel [137]. In contrast, a PEG-only transdermal photopolymerizable hydrogel (~10kPa) was used to encapsulate chondrocytes and implanted in nude mice [138]. After 7 weeks, collagen II production

and GAG deposition were detected in the hydrogel. Other synthetic polymers have been developed, such as a urethane-based prepolymer composed of (diisocyanato poly (ethylene glycol) and monohydroxl dimethacrylate poly (ε-caprolactone) triol, that can be photopolymerized to achieve a relatively high compressive modulus of ~110kPa [139]. However, little hydrolytic degradation was observed while enzymatic degradation occurred with 56 wt% over 28 days. After 8 weeks of culture, chondrocytes adhered to beads encapsulated in the polyurethane hydrogel deposited GAG and collagen II in both static and spinner flask culture [139].

One recent development in injectable cartilage tissue engineering is a scaffold-free approach, which presents the possibility of increasing the amount of therapeutic dose of cells by reducing the volume of polymer delivered. As described in previous sections, MSCs have been cultured as spheroids (100-500μm) that are small enough to pass through a needle without damage or loss of viability due to the shear force [93] and thus, can be used as an injectable cartilage tissue engineering strategy. Such approach is also attractive in the possibility of improving retention at the injection site compared to single cells. Additionally, material-based physical stimuli, such as microparticles, can still be incorporated and presented within the spheroids [140]. Due to its capacity for injectable delivery, ability to better mimic the physiological tissue structure [73] and maintenance of high differentiation potential, MSC spheroids cultured under chondrogenic conditions were investigated in this study.

Purpose of Thesis Project

The purpose of this project was to investigate the incorporation of CSMA microparticles in hMSC spheroids and how the presentation of the GAG within a

multicellular environment may affect chondrogenic differentiation. The first goal was to characterize the effects of CSMA microparticle incorporation on physical changes in the MSC spheroids. The incorporation efficiency of the microparticles was determined for a range of MP:cell number ratios. Analysis of MSC spheroid volume changes under chondrogenic culture conditions and the highest MP:cell number ratio (3:1) was also performed. General morphological effects of MP incorporation on the aggregates were studied with histological staining.

The second goal was to examine the extent of chondrogenic differentiation in hMSC spheroids and whether CSMA microparticles can promote MSC chondrogenesis in the presence of the exogenous cue TGF-β1. Microparticles have been cultured within multicellular aggregate in previous studies in order to introduce differentiation cues in a more uniform manner [90]. A number of studies have also investigated the effects of PLGA, PEG, and gelatin microparticles on the chondrogenic differentiation of larger MSC pellets [141-143]. However, chondrogenesis in small MSC aggregates containing microparticles has not been previously investigated. We have also demonstrated for the first time, the use of CS-based microparticles in the attempt to differentiate MSCs. Due to the ability of CS-based hydrogel scaffolds to promote chondrogenesis in MSCs [103, 104, 106, 144-146], we hypothesize that the incorporation of CSMA microparticles in the presence of TGF-β1 will more effectively promote cartilaginous ECM deposition and organization in hMSC spheroids. Specifically, MSC spheroids with or without incorporated CSMA microparticles were cultured in media containing soluble TGF-β1 for 21 days under hypoxia (3% O_2). MSC spheroids without MPs cultured in media without TGF-β1 served as a negative control. Changes in GAG deposition were analyzed

with histology. Gene expression of chondrogenic markers was determined with quantitative reverse transcription polymerase chain reaction and chondrogenic ECM protein production was confirmed by immunohistochemistry.

Portions of this chapter were adapted from Miller, T., Goude, M. C., McDevitt, T. C., & Temenoff, J. S. Molecular engineering of glycosaminoglycan chemistry for biomolecule delivery. *Acta biomaterialia*. 2013.

CHAPTER 2

MATERIALS AND METHODS

Chondroitin Sulfate Methacrylate Microparticle (CSMA MP) Fabrication

CSMA was synthesized by reacting chondroitin sulfate-A with methacrylic anhydride (Sigma-Aldrich) and sodium hydroxide in order to conjugate methacrylate groups to the native hydroxyl groups that are present on the N-acetylgalactosamine of the CS [146]. CSMA MPs of ~10μm diameter were prepared using a water-in-oil, single emulsion technique, as described previously [146]. CSMA (55.6mg) was dissolved in 440μL of PBS and mixed with ammonium persulfate (30 μL, 0.3 M) (Sigma-Aldrich) and tetramethylethylenediamine (30 μL, 0.3 M) (Sigma-Aldrich). The mixture was added dropwise to corn oil (60mL) with 2mL of Tween 20 and homogenized at 3,800rpm for 5 minutes. The mixture was then stirred and heated to 50°C under N_2 purging for crosslinking. After 30 minutes, the mixture was centrifuged at 3000rpm at 4°C to isolate the MPs. Following the removal of the corn oil, the MPs were washed 3 times with ddH_2O. Prior to incorporation in MSC spheroids, the MPs were incubated in 90% ethanol on the rotary at 4°C for 1 hour and washed with ddH_2O. The supernatant was removed from the MPs before lyophilization.

Chondrogenic Mesenchymal Stem Cell (MSC) Spheroid Culture

MSC Expansion

All cell culture reagents were acquired from Mediatech unless otherwise noted. Human bone marrow mesenchymal stem cells from 3 donors were obtained from the Texas A&M Health Science Center (Temple, TX). Passage 2 MSCs from each donor was

plated separately at low density (100 cells/cm^2) and expanded in growth medium composed of Minimal Essential Medium-alpha (α-MEM), 16.3% fetal bovine serum (Atlanta Biologicals, Lawrenceville, GA), 1% antibiotic/antimycotic and 1% L-glutamine until confluency under normixa (37°C at 5% CO_2 and 20% O_2). MSCs were then trypsinized and cells from all 3 donors were pooled prior to spheroid formation.

MSC Spheroid Formation

MSC spheroids were formed as previously described by forced aggregation using 400x400μm agarose microwell inserts [83, 90]. A single cell suspension of MSCs ($4.2x10^6$ cells/mL) was added to the microwell inserts and centrifuged at 200g for 5 minutes to deposit cells into the individual wells. The cells were incubated for 18 hours to allow aggregation under normoxia (37°C at 5% CO_2 and 20% O_2). The MSC spheroids were removed from the inserts using a wide-bore pipette for subsequent alginate encapsulation. MSC spheroids containing CSMA MPs were formed similarly; a pre-mixed suspension of MPs and cells (3:1 number ratio) was added to the agarose microwell inserts followed by a similar centrifugation and overnight incubation. Our previous study indicated that incorporation of MPs in embryonic stem cell aggregates at these MP:cell ratios was not detrimental to the maintenance of cell-cell contact or the distribution of MPs within the aggregate [147].

Spheroid Culture and Retrieval

After formation, MSC spheroids were suspended in 1.5% sodium alginate (Spectrum Chemical, Gardena, CA), which was crosslinked in a 100mm petri dish using a pre-cut filter paper (90mm diameter) to uniformly distribute 100mM calcium chloride (EMD, Darmstadt, Germany) across the surface, resulting in a thin layer (~1mm

thickness) that remained immobilized on the dish surface throughout the study. Alginate encapsulation was necessary to prevent agglomeration of MSC spheroids during extended culture periods (>4 days).

MSC spheroids suspended in alginate were cultured in serum-free medium containing high glucose Dulbecco's Modified Eagle Medium (DMEM), 1% non-essential amino acids, 1% antibiotic/antimycotic, 1% insulin, human transferrin, and selenous acid (ITS+) premix (BD Biosciences, San Jose, CA), 50μg/mL ascorbate-2-phosphate (Sigma-Aldrich) and 100nM dexamethasone (Sigma-Aldrich) under hypoxic conditions (37°C at 5% CO_2 and 3% O_2) for 21 days. For chondrogenic culture, 10ng/mL TGF-β1 (Peprotech, Rocky Hills, NJ) was added to the medium and is designated as +TGF-β in subsequent sections.

During culture the alginate layesr were dissociated with 55mM sodium citrate (Sigma-Aldrich, St. Louis, MO) and re-formed using the aforementioned method every 7 days of culture to minimize degradation of alginate. At experimental time points, the alginate layers were dissociated with sodium citrate and washed with phosphate buffer solution in order to collect samples for subsequent analysis at day 1, 7, 14, and 21.

Morphological and Chondrogenic Analyses

Spheroid Volume Analysis

MSC spheroids were imaged at day 1 and 21 using a phase contrast microscope (Nikon Eclipse TE2000-U, Tokyo, Japan). A minimum of 5 images with multiple spheroids per field (~10 spheroids/field) were taken for each experimental replicate. Spheroid diameters were measured using the ImageJ (v. 1.47) straight line selection tool

and used to calculate the volume, assuming perfect spheres. The volume data were normalized using the Box-Cox transformation prior to statistical testing [148].

Histological Staining

MSC spheroids were retrieved from the alginate hydrogels at day 1, 7, 14, and 21 and fixed in a 10% formaldehyde solution for 30 minutes for histological analysis. Fixed samples were immersed in 5% w/v sucrose solution (EMD, Darmstadt, Germany), before subsequently being replaced with increasing sucrose solution concentrations up to 15%, under vacuum (-25inHg). Samples were then vacuum-infiltrated with increasing concentrations of 20% sucrose:optimal cutting temperature compound (OCT) solutions (4:1 to 1:2 volume ratios). After overnight infiltration, samples were embedded in OCT and allowed to solidify for 10 minutes in a mixture of dry ice and 100% ethanol. Samples were stored at -80°C and cryosectioned at 10μm thickness (Thermo Scientific, Cryostar NX70) prior to staining with either hematoxylin and eosin (H&E) or Safranin-O.

Reverse Transcription Polymerase Chain Reaction (RT-PCR)

MSC spheroids were collected for gene expression on 1, 7, 14, and 21 days and lysed with RLT Lysis Buffer (Qiagen, Hilden, Germany). The cell lysates were further filtered with the QIAshredder tissue homogeneizer (Qiagen) and RNA was extracted with the RNeasy Kit (Qiagen). Reverse transcription was performed with iScript cDNA Synthesis Kit (Bio-Rad, Hercules, CA) using the T100 Thermal Cycler (Bio-Rad). Primers (Invitrogen) were custom designed to target human mRNA for *β-actin, SOX9, collagen II, aggrecan, collagen I, collagen X, myoD and runt-related transcription factor 2 (RUNX2)* as shown in Supplementary Table 1. Quantitative polymerase chain reaction (PCR) was performed using the SYBR Green Master Mix (Life Technologies). The raw

fluorescence data was first processed in LinReg PCR software to more accurately determine individual PCR efficiency and mRNA starting concentration (v13.1; http://www.hartfaalcentrum.nl) [149]. Fold regulation relative to the untreated Day 1 control was determined for each sample with 18S ribosomal protein and β-actin as endogenous housekeeping controls. The Box-Cox transformation was used to normalize the PCR amplification data of each gene for subsequent statistical analysis [148].

Table 1. Primer sequences of MSC gene markers

Target	Marker		Primer Sequences (5'→3')	GenBank
β-Actin	Housekeeping	*F* *R*	GCAGTCGGTTGGAGCGAGCATCCCC TCCCCTGTGTGGACTTGGGAGAGGAC	NM_001101
18S	Housekeeping	*F* *R*	CGATGGGCGGCGGAAAATAGCCTTTGC CAGTGGTCTTGGTGTGCTGGCCTCGG	NM_022551
SOX9	Chondrogenic	*F* *R*	GCGGAGGAAGTCGGTGAAGAACGGGCA TGTGAGCGGGTGATGGGCGGG	NM_000346
Collagen II (α1)	Chondrogenic	*F* *R*	ACCCCAATCCAGCAAACGTT ATCTGGACGTTGGCAGTGTTG	NM_001844
Aggrecan	Chondrogenic	*F* *R*	ACAGCTGGGGACATTAGTGG GTGGAATGCAGAGGTGGTTT	NM_001135
Collagen I (α2)	Fibroblastic	*F* *R*	GAAAACATCCCAGCCAAGAA GCCAGTCTCCTCATCCATGT	NM_000089
Collagen X (α1)	Hypertrophic Chondrocyte	*F* *R*	GGCCCAGCAGGAGCAAAGGG GTGGCCCGGTGGGTCCATTG	NM_000493
MyoD	Myofibroblastic	*F* *R*	GTCGAGCCTAGACTGCCTGT GTATATCGGGTTGGGGTTCG	NM_002478
RUNX2	Osteogenic	*F* *R*	GTGCAGAGTCCAGCAAAGGT AGCAGAGCGACACCCTAGAC	NM_199173

Immunohistochemistry

Immunostaining for ECM deposition in cryosectioned samples was performed using primary antibodies for type I, II, and X collagen, aggrecan, and α-smooth muscle

actin (α -SMA). Antigen retrieval was performed for all sections by incubating in 20 μg/ml proteinase K (Sigma-Aldrich) for 10 minutes at 37°C. Samples for aggrecan and collagen X immunostaining were deglycosylated with 0.75U/mL chondroitinase ABC (Sigma-Aldrich) for 1.5 hours at 37°C. Samples were blocked with Image-iT FX Signal Enhancer (Life Technologies, Carlsbad, CA) and incubated with the primary antibodies (for dilutions, see Supplementary Table 2) overnight at 4°C.Secondary antibody binding with Alexa Fluor 488-conjugated goat polyclonal anti-mouse immunoglobulin G (IgG, Molecular Probes, Carlsbad, CA) or IgM (Molecular Probes) was performed at room temperature for 1 hour. The samples were stained with Hoechst (Sigma-Aldrich) to visualize the nuclei. Isotype controls were similarly stained using a monoclonal mouse IgG1(Abcam) or IgM (Abcam) isotype antibody (data not shown).

Table 2. IHC antibody information

1° Antibody	Catalog Number	Isoform	Dilution	Deglycosylate
Aggrecan	Abcam (ab3778)	IgG	1:20	Y
α-SMA	Dako (IS61130-2)	IgG	None	N
Collagen I	Abcam (ab90935)	IgG	1:60	N
Collagen II	Abcam (ab3092)	IgG	1:20	N
Collagen X	Sigma (C7974)	IgM	1:20	Y
IgG Isotype	Abcam (ab91353)	IgG	1:10	N
IgM Isotype	Abcam (ab18401)	IgM	1:50	N

Statistical Analysis

A two-factor analysis of variance (ANOVA) with Tukey's *post hoc* multiple comparison test ($p \leq 0.05$) was performed on the data from the spheroid volume and RT-PCR analyses to determine statistical significance between samples using Minitab software (v15.1, State College, PA).

CHAPTER 3

RESULTS

Morphological Analysis

Effect of TGF-β and CSMA MPs on MSC Spheroid Size

The incorporation efficiency (~80%) of CSMA MPs in MSC spheroids was independent of the initial amount loaded up to 3:1 MP:cell number ratio (Fig. A1). The highest ratio (3:1) that yielded ~1,600 MPs per spheroid was used for this study in order to maximize any potential chondrogenic effects of the CSMA MPs without compromising the formation of the aggregate. Representative phase images from each culture condition are shown in Fig. 1. On day 1, there was no difference in volume between untreated spheroids and spheroids containing only MPs or TGF-β (Fig. 1I), but the +MP +TGF-β spheroids had the largest volume (0.009mm^3) and were almost 2 times larger than the other spheroids. After 21 days, the +MP +TGF-β spheroids had the largest volume (0.016mm^3) and were approximately 2 times greater than that of the +MP spheroids (~0.008mm^3) (Fig. 1J). The +TGF-β spheroids also exhibited slightly larger volume (~1.2x) than the +MP group. Regardless of MP incorporation, spheroids cultured in chondrogenic conditions experienced a greater increase in volume (~2-3x) compared to spheroids in non-chondrogenic conditions (~1.8-2x).

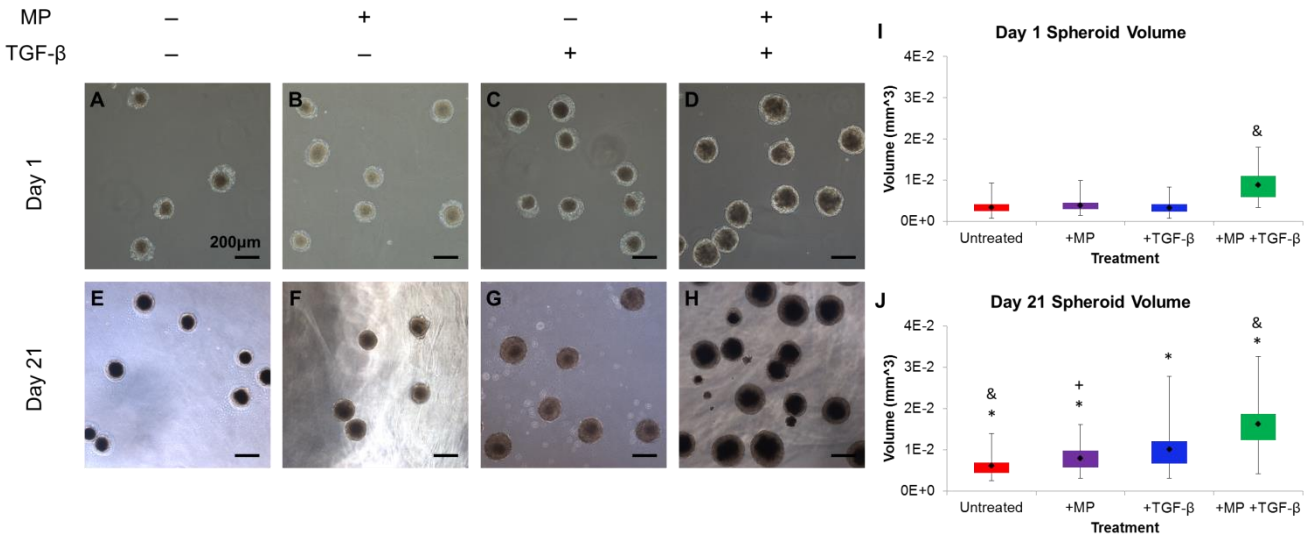

Figure 1. Changes in MSC spheroid volumes in response to MP incorporation and TGF-β. Differences in MSC spheroid sizes for each culture condition and over 21 days was observed in representative phase images (A-H). At day 1, the volume of +MP +TGF-β spheroids was significantly greater than all other groups (I). At day 21, the volume of all groups differed significantly from each other (J). $n_{population}$=3, $n_{spheroid}$=150, * indicates significantly different from same treatment at Day 1 ($p<0.05$). $^{+}$ indicates significantly different from the +TGF group ($p<0.05$). $^{\&}$ indicates significantly different from all other groups ($p<0.05$). Scale bar = 200µm.

CSMA MP Clustering and Morphological Changes in MSC Spheroids

Clustering of CSMA MPs near the center of the MSC spheroids was observed with or without TGF-β as early as day 7 in H&E staining (Fig. 2F, H, J, L). Particularly in the +MP +TGF-β spheroids, the cell nuclei exhibited pronounced elongation and circumferential alignment around the core of MPs at day 14 and 21 (Fig. 2H, L, arrows). The presence of GAG was detected in the ECM of +TGF-β spheroids at day 14 and 21 (Fig. 2S, W, arrows) by Safranin-O staining. GAG presence was also observed in the region of organized cells and ECM around the MP core in +MP +TGF-β spheroids at day 21 (Fig. 2X, arrows), but was absent in the +MP spheroids (Fig. 2V, arrows). Due to the lack of evident biochemical response of MSCs to the CSMA MPs without TGF-β, the +MP spheroids were omitted from subsequent analysis.

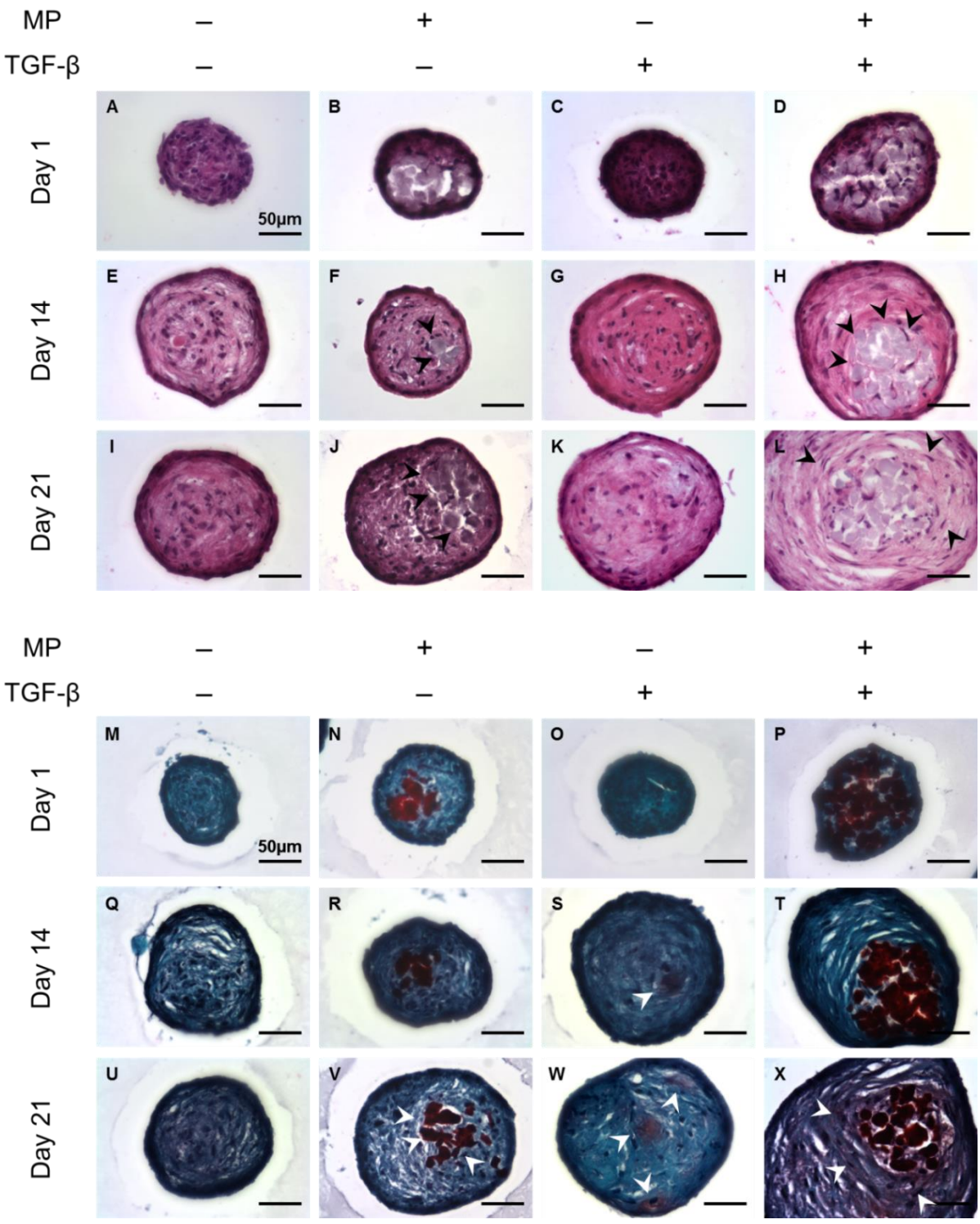

Figure 2. Histology shows differences in MSC spheroid morphology over 21 days. Cell morphology and organization changes in response to MP or TGF-β were observed in H&E staining (A-L). Presence of GAGs in the CSMA microparticles or in the ECM was confirmed by Safranin-O staining (red) (M-X). Fast green was used as a cytoplasm counterstain (M-X). n=3, scale bar = 50μm.

Chondrogenic Characterization

Increase in MSC Chondrogenic Gene Expression with TGF-β and CSMA MPs

Gene expression of the chondrogenic transcription factor SOX9 was significantly higher in the +MP +TGF-β spheroids (1.4±0.3 fold increase) than the untreated group at day 7, but decreased at day 21 (0.6±0.2) (Fig. 3A). The +TGF-β spheroids exhibited a gradual increase in the gene expression of aggrecan from day 7 to day 21 with a 6.7±0.7 fold increase at day 21 compared to the untreated (Fig. 3B). Similarly, collagen II expression in +TGF-β spheroids was increased at day 14 (1.6±0.7 fold increase) and day 21 (44±18 fold increase) (Fig. 3C). The +MP +TGF-β spheroids also demonstrated increases in aggrecan and collagen II gene expression, but the presence of the MPs resulted in earlier peaks (4.8±1.4 and 101±10 fold increase, respectively) by day 14 compared to the untreated spheroids.

In addition to promoting chondrogenic markers during differentiation, minimizing the expression of collagen I and X, which are indicative of the undesired fibrocartilaginous and hypertrophic phenotypes, is important. Collagen I expression was slightly increased by 1.5 fold at day 7 and sustained until day 21 in the untreated spheroids whereas in spheroids containing MPs and TGF-β, a 1.7 fold increase was not observed until day 14 (Fig. 3D). No significant change in collagen I gene regulation was found in the +TGF-β spheroids over time (Fig. 3D). The expression of collagen I was similarly elevated (~1.7 fold increase) in both the +MP +TGF-β and untreated spheroids at day 14. However, the presence of MPs in MSC spheroids with TGF-β resulted in a 0.6±0.1 fold decrease in collagen I expression at day 21 relative to the untreated group. For collagen X expression, the untreated spheroids demonstrated a gradual increase over

time, reaching a 5.7 fold increase at day 21 (Fig. 3E). In the +TGF-β spheroids, a 52 fold increase in collagen X regulation was observed by day 7 and sustained until day 21 (66±6 fold increase) while the addition of MPs in the spheroids promoted a large increase (81±17 fold increase) by day 14 followed by a sharp reduction at day 21 (12±3 fold increase). No significant difference in the elevated collagen X expression was detected between +TGF-β and +MP +TGF-β spheroids at day 14, but the addition of MPs resulted in slightly less pronounced increase compared to the untreated spheroids at day 21.

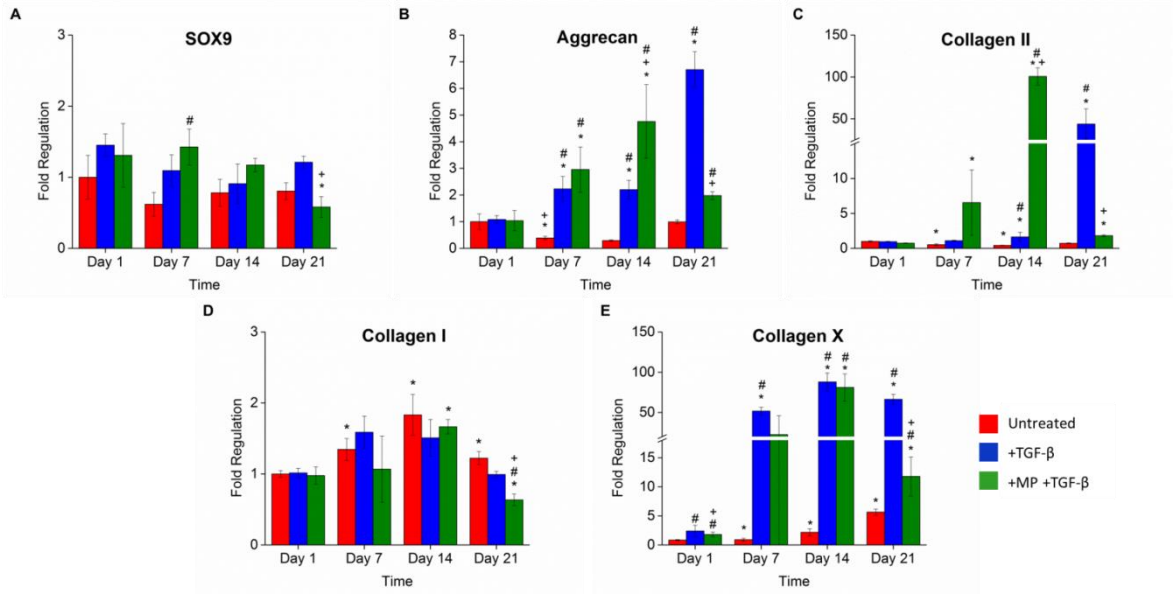

Figure 3. Expression of chondrogenic ECM gene markers by MSC spheroids in response to TGF-β and CSMA microparticles. Gene expression of SOX9 remained relatively constant over 21 days (A). The addition of TGF-β with or without CSMA microparticles promoted the expression of aggrecan (B) and collagen II (C) by day 7. Slight increase in collagen I expression was observed in all groups (D) while large increase in collagen X expression occurred in all except the untreated group (E). n=3, * indicates significantly different from same treatment at Day 1. # indicates significantly different from the untreated at the same time point. + indicates significantly different from the +TGF group at the same time point. All ($p<0.05$).

ECM Organization and Deposition in MSC Spheroids

At day 14, both groups cultured in TGF-β exhibited similar levels of increased staining for aggrecan compared to the untreated group (Fig. 4A-F). Collagen II staining was slightly stronger in the +TGF-β and +MP +TGF-β spheroids compared to untreated and there was no appreciable difference between the 2 groups (Fig. 4G-L). Collagen I appeared more organized in the +TGF-β spheroids and was distinctly aligned around the MP core in the +MP +TGF-β spheroids as compared to the amorphous staining in the untreated group (Fig. 4M-R, arrows). Some alignment of collagen X around the MP core could also be seen in the +MP +TGF-β spheroids compared to the other groups at day 14 (Fig. 4S-X, arrows). The presence of α-SMA could be detected strongly at the borders of the untreated and +TGF-β spheroids with some weak pericellular staining in the center (Fig. 4Y-DD). However, the addition of MPs in the presence of TGF-B greatly reduced the expression of α-SMA on the spheroid surface.

By day 21, organized pericellular staining of aggrecan was present around elongated nuclei in +TGF-β and +MP +TGF-β spheroids (Fig. 5A-F). Collagen II staining was high in +TGF-β spheroids, but slightly reduced with the incorporation of MPs (Fig. 5G-L). Similar amounts of positive staining for collagen I and X was observed in the +TGF-β and +MP +TGF-β spheroids (Fig. 5M-R, S-X). In the +MP +TGF-β spheroids, strong positive collagen I staining was observed on the periphery of the MP core and near the individual MPs at day 21 (Fig. 5O, R, arrows). Organization of collagen I around the MP core was still obvious after 3 weeks of culture and was also evident in collagen X staining (Fig. U, X, arrows). The presence of α-SMA on the spheroid surface

was observed in all groups, but the +TGF-β spheroids exhibited additional pericellular staining in the center compared to the +MP +TGF-β group at day 21(Fig. 5Y-DD).

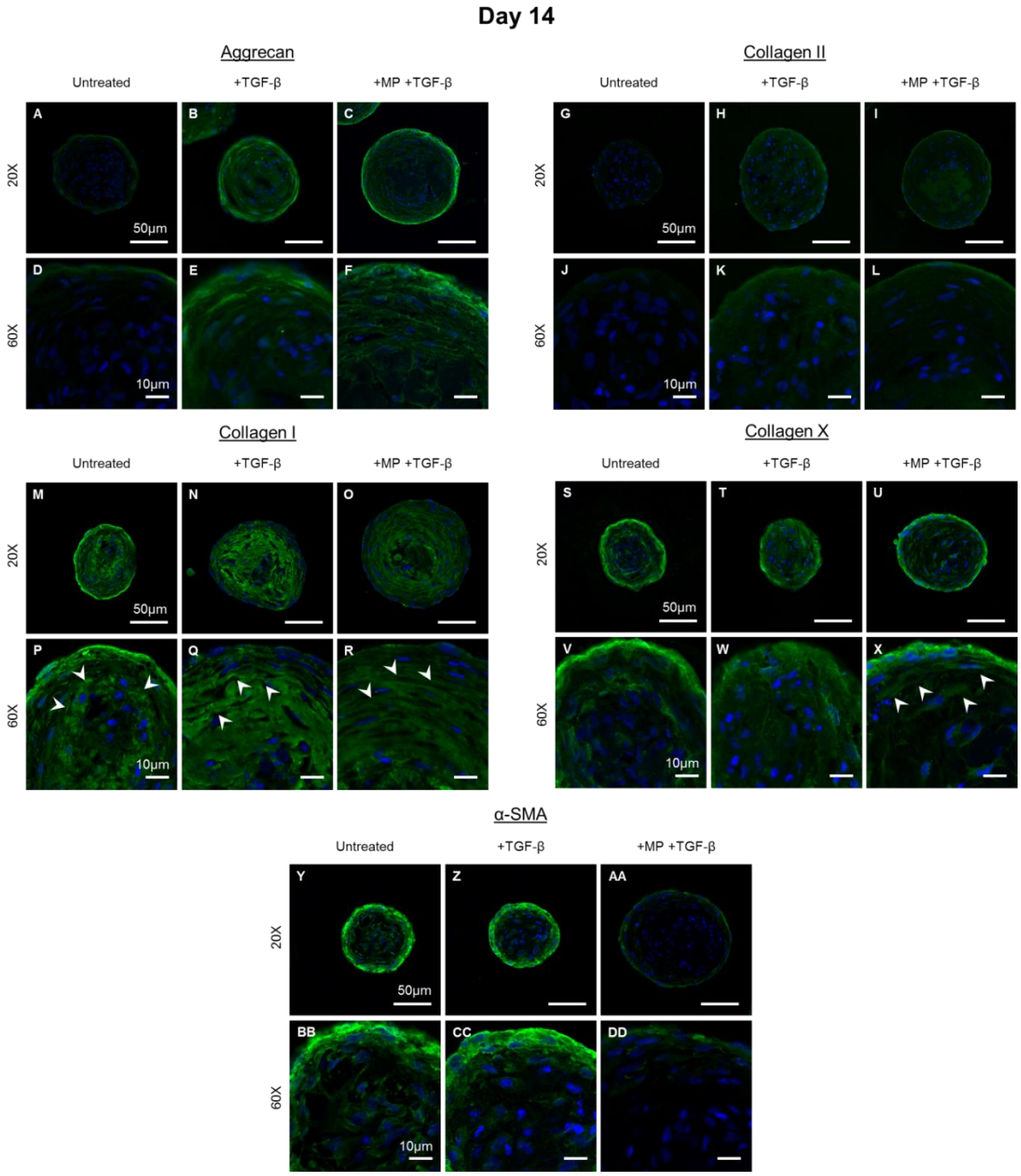

Figure 4. Immunofluorescence staining for deposition of chondrogenic ECM molecules in MSC spheroids at day 14. Positive aggrecan and collagen II staining were detected in all except the untreated group (A-F, G-L). Similar levels of collagen I and X were present in all groups (M-R, S-X) while differences were observed for α-SMA levels (Y-DD). Molecules of interest = green and cell nuclei = blue. n=3, scale bar=10μm.

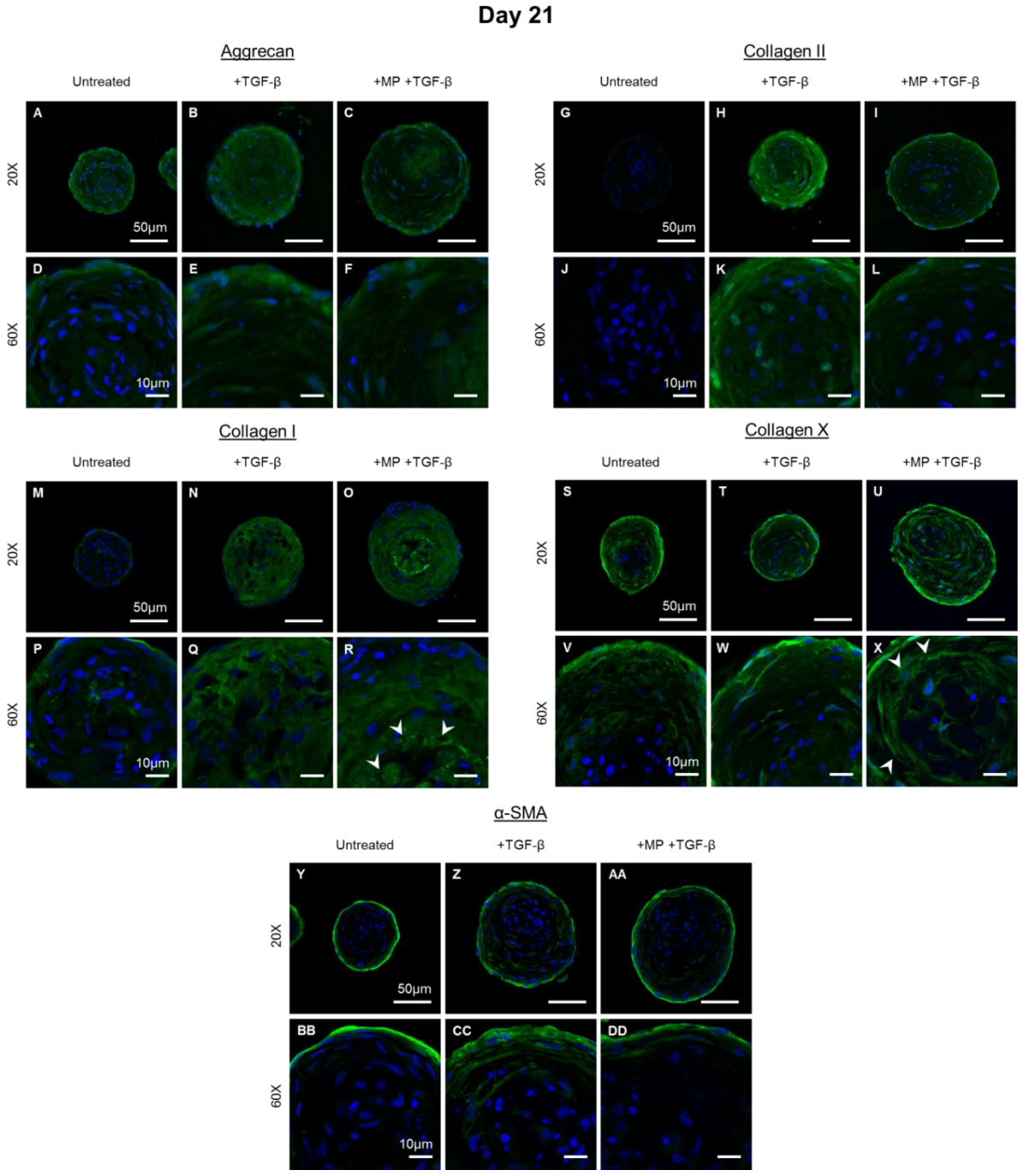

Figure 5. Immunofluorescence staining for deposition of chondrogenic ECM molecules in MSC spheroids at day 21. Positive staining for aggrecan was detected in all groups, but collagen II staining was still absent in the untreated group (A-F, G-L). Collagen I levels in the untreated spheroids was low, but collagen X staining was similar between all groups (M-R, S-X). α-SMA staining was also observed across all culture conditions (Y-DD). Molecules of interest = green and cell nuclei = blue. n=3, scale bar=10μm.

A comparison between day 14 and 21 IHC showed no appreciable changes in the amount of aggrecan staining detected in +TGF-β spheroids or in +MP+TGF-β samples.. Collagen II appeared to increase in +TGF-β spheroids over time, while little change was seen in the +MP +TGF-β spheroids. No difference was observed in collagen I and X staining between day 14 and 21 in +TGF-β spheroids or in +MP +TGF-β spheroids., An apparent reduction in the area of positive α–SMA staining on the surface of untreated and +TGF-β spheroids along with decreased pericellular staining in the center occurred between days 14 and 21. Although the +MP +TGF-β spheroids exhibited a slight increase in the presence of α–SMA on the surface between days 14 and 21, the amount of α–SMA presentat day 21 was still comparable to that of +TGF-β spheroids.

CHAPTER 4

DISCUSSION

Morphological Analysis

We have demonstrated the ability to incorporate GAG-based MPs in hMSC spheroids for chondrogenic differentiation in this study. Specifically, MSC spheroid volume was significantly enhanced by the combination of CSMA MPs and TGF-β, which also exhibited a unique organization of cells and ECM around the MP core. Some evidence of earlier chondrogenic differentiation in the spheroids with MPs was observed at the gene expression level (aggregan and collagen II), although all samples with TGF-β treatment exhibited similar levels of GAG, aggrecan, collagen I, II, and X staining by 14 days of culture. From the spheroid size analysis, the +MP +TGF-β spheroids were found to exhibit the largest volume at both days 1 and 21. Part of this large increase in volume could be attributed to the presence of the MPs. However, calculating the sum of theoretical total MP volume and the volume of a spheroid alone cultured in TGF-β at day 1 and 21 still resulted in a ~20% and ~30% lower values, respectively, than that measured in the +MP +TGF-β spheroids, which indicates that the combination of CSMA MPs and TGF-β has more than a purely additive effect on the volume of MSC spheroids. In a comparable hMSC spheroid system without exogenous growth factors, size difference between spheroids with or without gelatin MPs was not observed at day 1 nor was any increase seen up to 7 days of culture [80].

The incorporation efficiency for CSMA MPs was close to 100% for all three MP:cell ratios investigated (Fig. 1S), suggesting that the MSCs may have an affinity for and can easily interact with CS-based materials. As noted in a study in which PLGA,

agarose or gelatin MPs were incorporated in embryonic stem cell aggregates, differences were observed in incorporation efficiencies, which was attributed to the difference in material adhesiveness [90]. In addition to high incorporation, the CSMA MPs spontaneously clustered within the MSC spheroids by day 7 and remained as a core for the duration of the culture as shown by histology, which was not observed with polystyrene (PS) MPs (Fig. S2), even though, in this system, the PS microparticles had similar incorporation efficiencies as CSMA MPs (data not shown). Clustering of MPs in MSC pellet culture containing PEG, PLGA, or gelatin MPs has not been previously reported [141-143]. In previous studies, the diameters of the MPs ranged from ~6-7μm (PEG and PLGA) [141, 142] to ~15μm (gelatin) [143], which are comparable to the size of the CSMA MPs (~10μm). Because PLGA and PEG are synthetic materials, it might be expected that MSCs may interact with them differently than with the CS-based MPs. However, clustering was also not observed in MSC pellets that included gelatin particles when cultured up to 4 weeks [143]. Together with the volume analysis data, this suggests that there may be further interactions of MSCs specifically with CS-based particles that allow their movement and rearrangement in the spheroids after formation. Such interactions may affect overall cellular or ECM packing in the spheroids [143], that leads to a larger overall spheroid volume in the presence of TGF-β, even after only 1 day.

While further studies are required to better understand the nature of any specific MSC–CSMA MP interactions in this system, it was observed that the MSC spheroids exhibited uniform circumferential organization of elongated cell nuclei and ECM around the clustered MP core as seen in the H&E (Fig. 2H, L) and IHC staining (Fig. 4R, X, 5R, X), particularly in the presence of TGF-β. Chondrocytes adopt a fibroblast-like

morphology with a spread and elongated appearance in monolayer culture on two dimensional substrates [150]. Concomitant with the loss of a rounded phenotype, chondrocytes de-differentiate and decrease expression of aggrecan and collagen II, while increasing production of collagen I [151-154]. While de-differentiation may be a concern in this system due to the elongated cell morphologies observed in the +MP +TGF- β samples, no evidence was observed via gene expression analysis or IHC that would suggest this was occurring overall in these samples. Instead, the unique organization around the MP core has not been reported in previous pellet or spheroid and MP systems and presents a possible avenue for directing microtissue radial architecture from the inside-out to more closely mimic the zonal organization of tissues such as articular cartilage [5].

To better understand the potential effects of this MP core on cellular organization, staining for α-SMA was performed. TGF-β1 has been shown to increase the α-SMA expression and contractility in human MSCs at 1ng/mL [155] and α-SMA production has also been detected in the outer region of MSC pellets [142, 155]. We saw a similar pattern of expression near the surface of all spheroids, which suggests that α-SMA expression may have resulted from the contractility exerted by the MSCs near the surface of the spheroid. Interestingly, there was a pronounced reduction of α-SMA protein on the border of +MP +TGF-β spheroids at day 14, showing that the CSMA MPs may have the ability to prevent TGF-β from inducing α-SMA expression mechanically by acting as a substrate that modulates cell contractility [155, 156]. A similar reduction of α-SMA staining from the border was seen in MSC pellets containing PEG MPs cultured in TGF-β3-supplemented media [142], further indicating that the physical presence of MPs may

play an important role in mediating α-SMA production, possibly by disrupting cell-cell and cell-ECM interactions.

Chondrogenic Characterization

One of the problems with *in vitro* chondrogenic culture is potential hypertrophy, so the use of hypoxic culture is necessary to mitigate the undesired phenotype [55, 57, 58]. The oxygen tension for chondrogenic culture has typically ranged from 1 to 5% O_2 [55-58], and, accordingly, the experiments in this study were performed at 3% O_2. Although the +MP +TGF-β spheroids displayed similar levels of increased expression for chondrocytic genes (aggrecan and collagen II) as the +TGF-β spheroids, the +MP +TGF-β spheroids showed highest expression levels 1 week earlier than the +TGF-β group for collagen II and aggrecan (Fig. 3B, C), which suggests that the CSMA MPs play a role in mediating the temporal sequence of TGF-β-induced chondrogenesis. CS has been shown to electrostatically interact with positively charged growth factors, such as TGF-β, and to modulate growth factor signaling during cartilage morphogenesis [157], so it is possible that the MP core could mediate the quantity and distribution of TGF-β1 available to induce differentiation in our culture system, resulting in the earlier expression of cartilaginous genes by MSCs. We also noted that gene expression of negative lineage marker RUNX2 (osteogenic) was minimally increased in all spheroids over 21 days (Fig. S3A) and myoD (myofibroblastic) was decreased in all groups over 21 days (Fig. S3B).

In order to determine the degree and location of deposition of each of ECM molecules tracked with RT-PCR, IHC staining was used. In contrast to the gene expression data, which indicated earlier onset of differentiation for the MP laden group, both sets of TGF-β treated spheroids (with or without MPs) exhibited similar levels of

staining for aggrecan and collagen II protein deposition at day 14 and 21 (Fig. 4 and 5E, F, K, L). In addition, GAG staining for +TGF-β spheroids was observed earlier than the +MP +TGF-β group (Fig. 2W, X). Other hMSC pellet culture in hypoxia has also found increases in collagen II and aggrecan gene expression that was not reflected in protein production [158]. Increased expression and/or activity of proteases, in the +MP +TGF-β spheroids may provide another potential explanation for the difference.

As mentioned previously, in addition to enhancing chondrogenic gene and ECM markers, another goal of *in vitro* MSC chondrogenesis is to minimize fibrocartilaginous and hypertrophic phenotypes, which can be detrimental for long-term articular cartilage restoration [53, 54]. Fibrocartilaginous collagen I gene expression was slightly elevated with spheroids cultured in TGF-β1 (Fig. 3D) similar to the increase seen in smaller micropellets under hypoxia [70]. Moreover, strong positive IHC staining was observed throughout the ECM at all timepoints in the spheroids as seen in hMSC micropellets [70] and larger MSC pellets without MPs [45, 70] or with PEG [142] and gelatin MPs [143]. Despite the reported ability of hypoxic culture to delay or suppress hypertrophy in pellets or encapsulated MSCs [55, 57, 58], ~80 fold increase in collagen X gene expression at day 14 found in TGF-β-treated spheroids with or without MPs was confirmed by IHC staining (Fig. 3E). Even under hypoxic conditions, increases in collagen X levels during chondrogenesis have still been reported in MSCs cultured in various formats [68-70], which demonstrates the difficulty in preventing hypertrophy *in vitro*. Mixed results were observed in previous work with MSC pellets containing MPs, where the incorporation of gelatin MPs led to collagen I mRNA levels similar to those seen in no MP controls [143], but PEG MPs reduced both collagen I and X gene expression [142]. These findings show

varying levels of effectiveness in suppressing collagen I and X expression between each study, which implies that other factors, such as aggregate size and MP type, may play a role in modulating MSC phenotype. Thus, culture conditions for our specific system may need to be further optimized to reduce the fibroblastic and hypertrophic differentiation of MSCs.

While the gene expression results are intriguing, it does not appear that the presence of the CSMA MPs enhanced deposition of cartilaginous ECM in this spheroid culture. There could be several explanations for this, including that the MP dose was not appropriate for differentiation, and that there was minimal degradation of the CSMA MPs observed in the MSC spheroids over 21 days. While the MP:cell ratio was chosen to allow sufficient cell-cell contact to form spheroids while still incorporating sufficient GAG in the system, on a per cell basis, the concentration of CS in the spheroid is similar to the physiological concentration in the articular cartilage of the knee according to our calculations (data not shown). Despite the large number of CSMA MPs present within a spheroid, only a number of MPs on the surface of the core would be available for direct cell-GAG interaction, thus reducing the overall "dose" of GAG compared to CS-based hydrogels with encapsulated hMSCs, which contained ~6-10x higher amount of GAG per cells than native cartilage [144, 159]. The CSMA MPs induced similar levels of chondrogenesis as these CS-based hydrogels even at a lower "dose" of GAG, suggesting that the organization of the MPs, MSCs, and ECM within the aggregate may help maintain the chondrogenic differentiation potential as spheroid culture has been shown to preserve the ability of MSCs to commit to adipogenic and osteogenic lineages [80]. There was also little degradation seen in the MPs over the course of the experiment,

which, in addition to non-uniform distribution of CS within the spheroid, would likely minimize release of any sequestered growth factors. In the future, the introduction of groups into CSMA MPs that promote degradation may allow a more homogeneous distribution of GAGs and sustained release of any sequestered growth factors through the duration of the culture to better promote chondrogenesis, as has been explored previously with degradable gelatin and PLGA MPs in MSC pellets [141, 143]. Alternatively, the use of smaller CSMA MPs in the spheroids may also promote more uniform dispersal throughout the aggregate ECM as seen in the incorporation of PLGA MPs (1-11μm diameter) in embryonic stem cell aggregates [160] or the addition of RGD sequences in CSMA to enable direct cell attachment to MPs. Together, such a spheroid system would more closely mimic the native ECM by achieving a more homogeneous distribution of GAGs among cells [161] rather than being localized to a part of the pellet/spheroid.

CHAPTER 5

CONCLUSION

In these studies, we have demonstrated that the incorporation of CSMA MPs in hMSC spheroids did not adversely affect TGF-β1-mediated chondrogenesis and that MPs promote earlier gene expression of chondrogenic markers compared to spheroids without MPs. In addition, the clustering of CSMA MPs resulted in unique cellular and ECM alignment in the MSC spheroids that may provide a means to spontaneously form areas of high alignment within microtissues. As GAGs are found in a wide variety of tissue types, such results indicate that this culture system can serve as a novel platform both to further examine the effects of GAGs and growth factors on MSC phenotype, as well as potentially direct differentiation in a more spatially controlled manner that better mimics the architecture of specific target tissues.

APPENDIX A

SUPPLEMENTARY FIGURES

CSMA MP Incorporation Efficiency Analysis

Materials and Methods

Following the aforementioned MSC spheroid formation technique, CSMA microparticles were incorporated in the MSC spheroids at 1:3, 1:1, and 3:1 MP:cell number ratios. Samples were collected on day 1 after formation for Safranin-O staining using the same histological procedure in this study. After the number of spheroids per sample was determined, the MSC spheroids were dissociated by incubating in 0.25% trypsin for 1 hour at 37°C (5% CO_2 and 20% O_2). To isolate the MPs from the dissociated MSCs, 5% sodium dodecyl sulfate (SDS) was then added to the cell-MP suspension for 5 minutes. The number of MPs was determined on a hemocytometer and divided by the number of MSCs based on the previous spheroid count to determine the experimental MP:cell ratio.

Results

Difference in the amount of MPs incorporated in the MSC spheroids can be observed compared to the no MP control (Fig. A1A-D). The incorporation efficiency of the CSMA MPs was quantitatively assessed for a range of MP:cell number ratio (1:3, 1:1, and 3:1), which showed that nearly all of the MPs loaded become incorporated within the spheroids after formation (Fig. A1E).

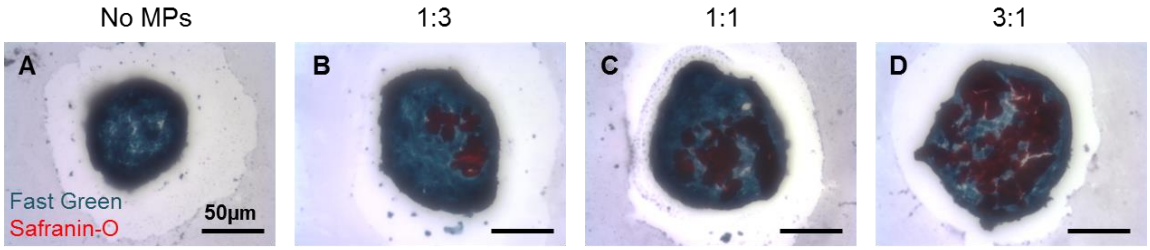

E

MP:Cell (loaded)	MP:Cell (retrieved)
0.3 (1:3)	0.3 ± 0.04
1 (1:1)	1.2 ± 0.1
3 (3:1)	2.4 ± 0.7

Figure A1. Efficiency of CSMA microparticles incorporation in MSC spheroids. Increasing amounts of CSMA microparticles (red) incorporated in the MSC spheroids was shown by Safranin-O staining (A-D). The theoretical loaded MP:cell ratios corresponded closely to the ratio evaluated by spheroid dissociation and MP retrieval (E). n=3, scale bar=50µm.

CSMA MP Clustering Effect

Materials and Methods

MSC spheroid formation and MP incorporation was done using the same protocol detailed in this study. CSMA MPs were added at to the MSC cell suspension at a 3:1 MP:cell ratio and the polystyrene MPs were added at a 6:1 ratio to achieve comparable numbers of incorporated MPs in the spheroids due to a lower incorporation efficiency. The spheroids were cultured in the same chondrogenic conditions under hypoxia in alginate layers and collected at day 1 and 7 for processing using the same histological procedure described previously without the application of any stains. The spheroids were then imaged using a phase contrast microscope.

Results

At day 1, a random distribution of both CSMA and polystyrene MPs was observed in the MSC spheroids (Fig. A2A, C). However, the CSMA MPs became organized into a cluster in the center of the spheroid by day 7 with distinct organization around the MP core (Fig. A2B). In contrast, the polystyrene MPs remained distributed across the spheroid ECM without any pronounced rearrangement, indicating possible difference in the cell-material interaction (Fig. A2D).

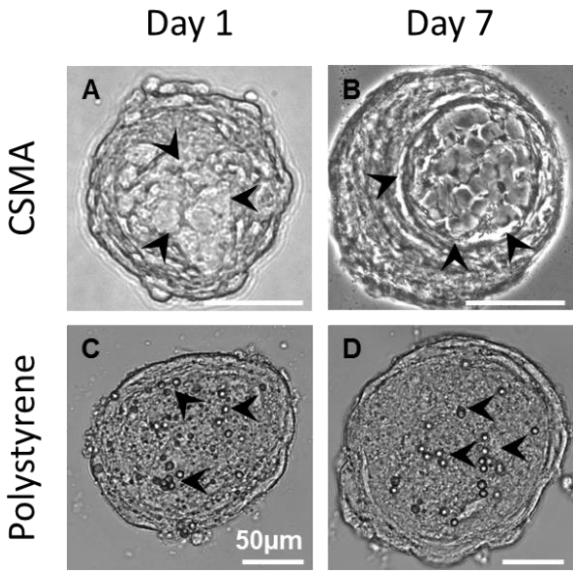

Figure A2. CSMA microparticles cluster by day 7 in hMSC spheroids. CSMA (A) and polystyrene (C) microparticles were distributed throughout the spheroids on day 1 (arrows). However, the CSMA microparticles aggregated after a week of culture (B), whereas the polystyrene microparticles remained spread across the spheroid (D). n=3, scale bar=50µm.

Negative Lineage Marker Gene Expression

Materials and Methods

Quantitative RT-PCR was performed using the SYBR Green Master Mix using the same procedure for the gene expression analysis in this study. The raw fluorescence data was also processed in LinReg PCR software and normalized by Box-Cox transformation prior to statistical analysis with ANOVA. Fold regulation relative to the untreated Day 1 control was also determined for each sample with 18S ribosomal protein and β-actin as endogenous housekeeping controls.

Results

Less RUNX2 expression was detected in +MP +TGF-β spheroids at day 21 compared to +TGF-β spheroids (Fig. A3A) and both +TGF-β and +MP +TGF-β spheroids demonstrated reduced MyoD expression compared to the untreated group for all time points (Fig. A3B).

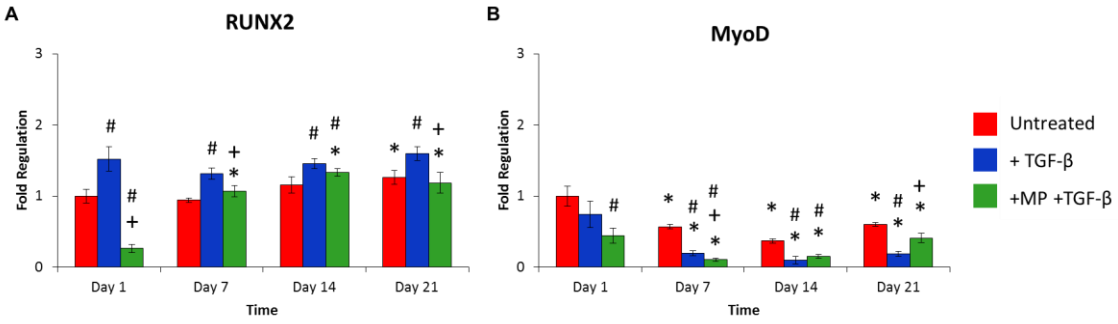

Figure A3. Gene expression of negative lineage markers in MSC spheroids. RUNX2 expression was sustained from day 7 to 21 in all groups (A) and MyoD expression was decreased over 21 days in all groups (B). n=3, * indicates significantly different from same treatment at Day 1 ($p<0.05$). $^{\#}$ indicates significantly different from the untreated at the same time point ($p<0.05$). $^{+}$ indicates significantly different from the +TGF group at the same time point ($p<0.05$).

Microabrasion Cartilage Defect Model

Materials and Methods

The Gold Series MegaPeel microdermabrasion machine (DermaMed USA, Lenni, PA) with the gold handpiece assembly from the Prausnitz laboratory was used for microabrasion of articular cartilage. By sealing the opening on the plastic tip of the handpiece, vacuum forms and drives the flow of the silica crystals from the machine to the target surface. During abrasion, the tissue debris and crystal circulate in the plastic tip and are directed back into a closed waste container. The crystal flow rates have been previously determined by Andrews, et al. to range from 8.9×10^{2} to 2.2×10^{5} particles/s and the suction pressure from 30 kPa to −60 kPa [162]. The flow rate was adjusted to the maximum setting ("9" on the dial), which corresponded to roughly 10^{5} particles/s, for cartilage microabrasion [162]. Microabrasion masks were made from stainless steel sheets (75μm thickness, Trinity Brand Industries, Countryside, IL) by Vladimir Zarnitsyn, PhD from the Prausnitz laboratory. Holes (120, 250, 275μm diameters) were patterned on the masks using AutoCAD software (Autodesk, San Rafael, CA) and an infrared laser (Resonetics Maestro, Nashua, NH).

Femur and tibia were harvested from calf legs (Research 87, Marlborough, MA) while intact hind legs were retrieved from practice rats for microabrasion on the articulating joint surface. To abrade the bovine cartilage, the handpiece was positioned so that the tip opening was flush against a rubber seal that sits above the cartilage surface as seen in Fig. A4. The length of the microabrasion ranged from 3, 6 to 12 minutes. Abrasion with and without the stainless steel masks, which were inserted between the rubber seal and cartilage surface as shown, were also tested. The abraded bovine cartilage

was removed from the respective femur or tibia with a scalpel. Another piece of cartilage was removed from the vicinity as unabraded controls. The samples were infiltrated with OCT-sucrose solutions as described previously before embedding and cryosectioning at 10μm thickness. Alcian blue was used to visualize surface defects.

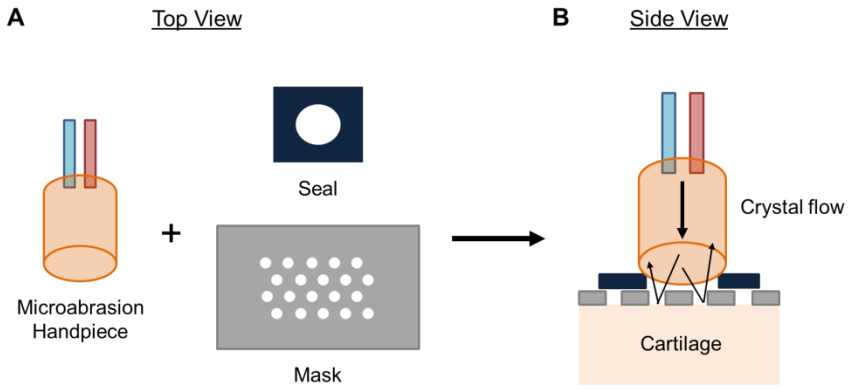

Figure A4. Cartilage microabrasion schematic. The microabrasion handpiece was used in conjunction with a rubber seal and stainless steel mask to abrade cartilage (A). The handpiece was placed on top of the seal above the cartilage. When the mask was in use, it was inserted between the rubber seal and the cartilage surface (B).

The medial condyles of harvested rat femurs were similarly abraded without the mask and the lateral condyles from the same joint served as unabraded controls. In intact rat legs, the femoral groove required surgical isolation prior to microabrasion. An incision was first made along the length of the medial side of the patellar tendon (Fig. A5A). The knee was flexed and the patellar tendon was dislocated laterally to expose the femoral groove for microabrasion as seen (Fig. A5B). Similar to the microabrasion of bovine cartilage, the handpiece was immobilized over the target tissue on top of the rubber seal with or without the stainless steel mask (Fig. A5C). After the abrasion, the femur was harvested and incubated in 1% protease inhibitor cocktail (CalBiochem, San Diego, CA) and ionic contrast agent Hexabrix 320 (Mallinckrodt, Hazelwood, MO) solution for 1 hour. The abraded femurs were imaged in a 12mm scanning tube with μCT

40 (Scanco Medical, Bassersdorf, Switzerland) at 45kVp, 177µA, 200ms integration time and a voxel size of 12µm [163]. Using the equilibrium partitioning of an ionic contrast agent (EPIC) technique [163], the cartilage morphology and proteoglycan composition of the abraded joints were determined.

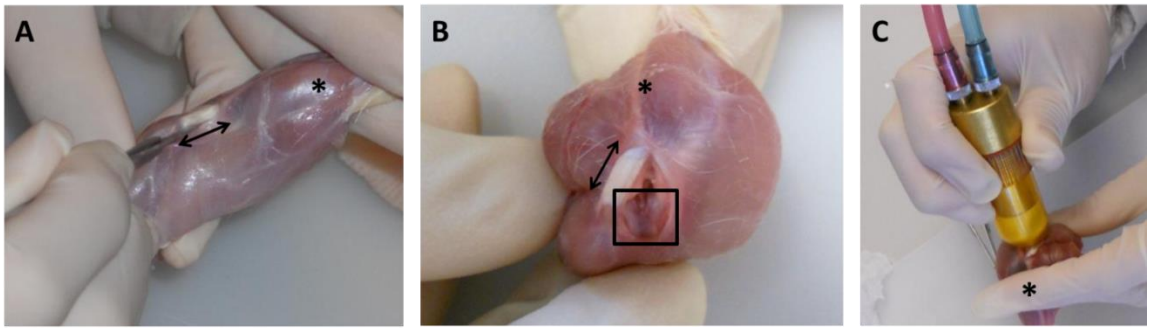

Figure A5. Isolation of rat femoral groove for microabrasion. An incision was made along the medial length of the patellar tendon (black double-ended arrows) (A) in order for the femoral groove (black box) to be exposed in the flexed joint (B). The handpiece was then placed over the exposed cartilage for microabrasion (C). * indicates the distal end of the joint.

Results

The Gold Series MegaPeel microdermabrasion system has been previously characterized for controlled abrasion of porcine skin [162]. The process was adopted for the development of a cartilage defect model with some modifications. Due to the curvature of the cartilage surface, a rubber seal was used to better maintain the vacuum between the handpiece and the target tissue. The stainless steel masks were added with the goal of creating a pattern of focal defects in the cartilage. The microabrasion process was initially tested on bovine cartilage and later refined for intact rat joints.

The superficial zone of bovine cartilage was removed after 3, 6, and 12 minutes of microabrasion without the mask compared to the unabraded controls (Fig. A6A-F). However, the amount of tissue abraded from the surface did not appear to increase with the length of microabrasion time. Bovine cartilage was also abraded for 12 minutes with

the stainless steel mask of 125µm diameter holes. However, large variations in the size and morphology of surface defects created by the microabrasion process were observed between samples (Fig. A7D-F).

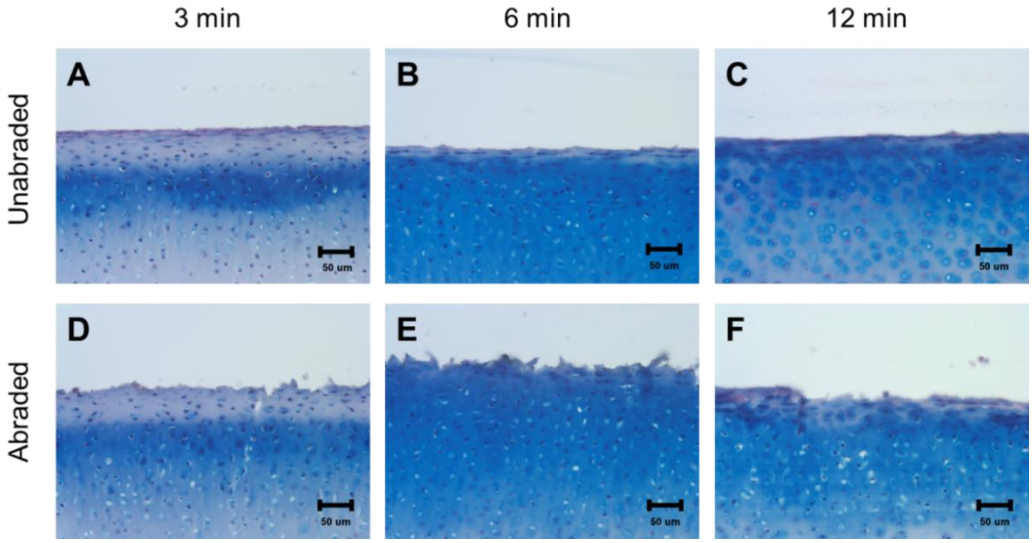

Figure A6. Surface fibrillation in bovine cartilage after 3, 6 or 12 minutes of microabrasion. Unabraded cartilages exhibited an intact superficial zone (A-C) while abraded samples showed similar loss of tissue at the surface (D-F) independent of microabrasion time. Scale bar = 50µm.

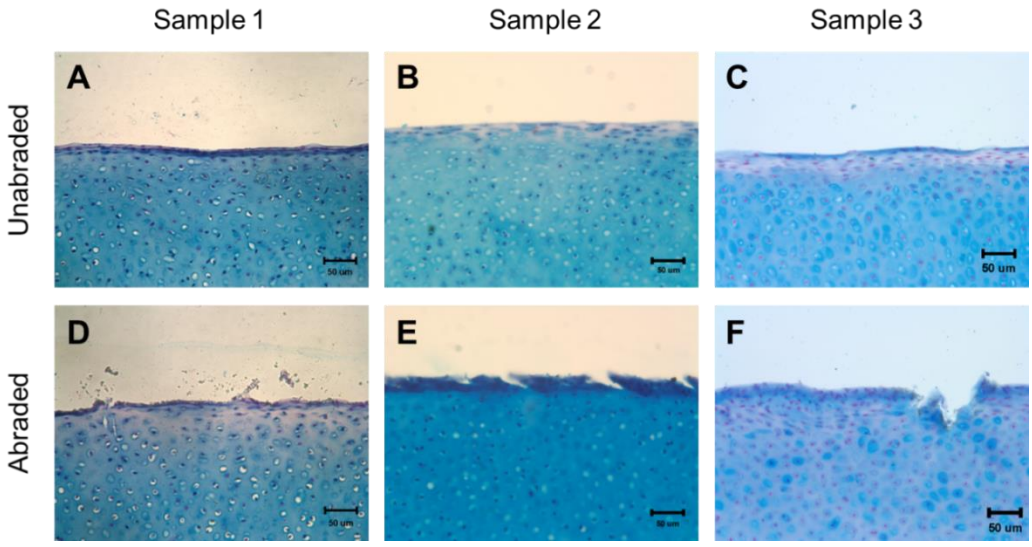

Figure A7. Variable surface fibrillation in bovine cartilage after 12 minutes of abrasion with mask (125µm diameter holes). The superficial layer of unabraded cartilage remained intact (A-C). Some surface disruption was seen in sample 1 (D) while sample 2 exhibited a pattern of lesion (E) and sample 3 showed a focal defect (F). Scale bar = 50µm.

Some surface roughness and flattening was observed in all of the abraded rat condyles with μCT (Fig. A8A-D, arrows). The cartilage thickness quantified by EPIC was lower for the abraded condyle compared to the unabraded control for all abrasion time (Fig A8E). Higher attenuation values were generally observed in the abraded condyles, which corresponded to lower GAG content that may signify loss of cartilage tissue.

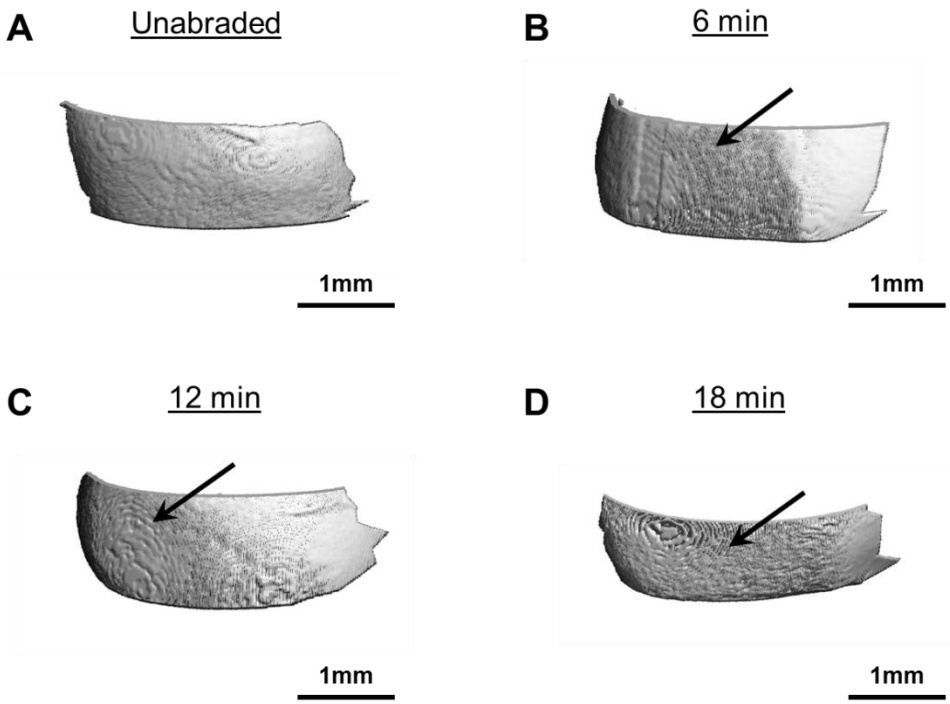

E

Abrasion Time (min)	Unabraded	6	Unabraded	12	Unabraded	18
Cartilage Thickness (mm)	0.045	0.044	0.047	0.036	0.043	0.032
Attenuation (mg HA/ccm)	637.1	625.4	575.2	707.7	620.1	755.4

Figure A8. Microabrasion of rat condyles visualized and quantified by μCT. Disruption to the articular cartilage surface were observed for all abrasion times (B- D) compared to the unabraded control (A). Quantitative analysis showed reduced cartilage thickness after abrasion along with increased attenuation values (E). Scale bar = 1mm, n=1.

Similarly, surface roughness could be seen in the rat femoral grooves that were abraded for 6 and 9 minutes. The area of abrasion extended across the entire width of the femoral groove and in patellar surface in the 6 min sample (Fig. A9B, arrow), whereas the pattern of abrasion mainly localized along the grooves in the 9 min sample (Fig. A9C, arrows). The difference in the abrasion pattern may be partially contributed by the difficulty in positioning the handpiece and seal tightly against the curvature of the groove. Because the thickness of rat cartilage is much lower than that of bovine cartilage, microabrasion for 12 minutes resulted in the complete erosion of the tissue (Fig. A9D, arrow). Reduction of abrasion time and the use of stainless steel mask still need to be further investigated in the rat cartilage model.

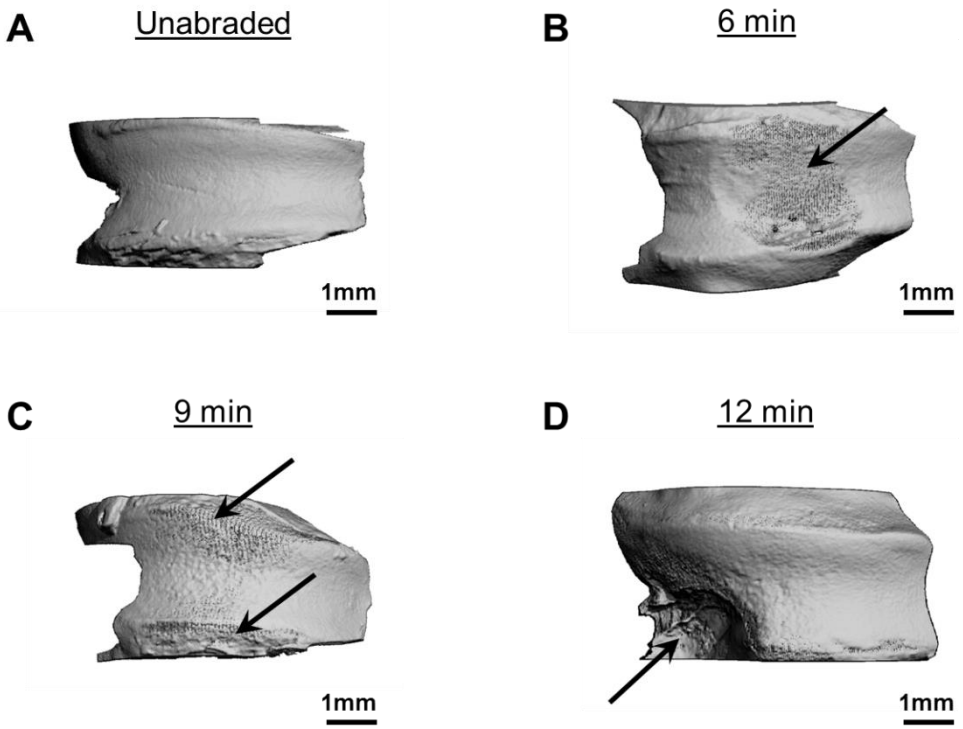

Figure A9. Microabrasion of the rat femoral groove. Abrasion for 6 and 9 minutes induced visible surface roughness (B, C). However, 12 minutes of abrasion caused the complete removal of cartilage from the groove (D). Scale bar = 1mm, n=1.

Microdrilling Cartilage Defect Model

Materials and Methods

Cartilage Explant Harvest

Bovine femur was similarly harvested from fresh calf legs as previously described. David Reece from the Guldberg Lab contributed greatly to the development of the microdrilling procedure. Prior to microdrilling, the bovine femur was immobilized on the stereotaxic instrument (David Kopf Instruments, Tujunga, CA) as seen in Fig. A10. A dissecting scope was used to visualize the tip of the 0.25mm diameter microdrill bit (Midwest Circuit Technology, Aurora, OH) and to position it perpendicularly and flush against the condyle cartilage surface that has been pre-marked in 6mm diameter circles. A pattern of ten microdefects 100μm deep and 1mm apart was achieved within the 6mm diameter circles. The cartilage was then excised from the condyle by cutting along the pre-marked boundaries with a scalpel to obtain a relatively circular explant with a few millimeters in thickness. For histology, the cartilage explants was first fixed in 10% formalin. The surface of the explants was stained with Alcian Blue in order to visualize the defects.

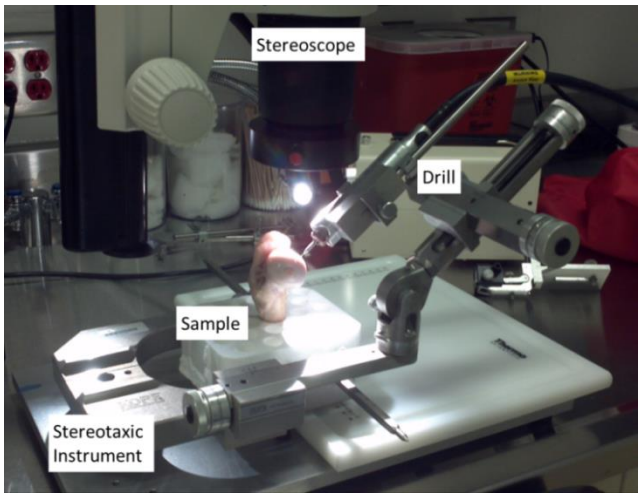

Figure A10. Bovine cartilage microdrilling setup. The bovine femur was fixed to a styrofoam block and immobilized on the stage of the stereotaxic instrument. The stereoscope was then positioned over the articular cartilage to visualize the drill bit during the microdrilling procedure.

CS-NHS Conjugation

The protocol of CS-NHS conjugation was developed by Torri Rinker. One liter of 95% ethanol was first chilled at -20°C. A 10% (w/v) chondroitin sulfate-C (463.369 g/mol), a 25% (w/v) N-hydroxysuccinimide (NHS) (115.087 g/mol) and a 67% (w/v) N-(3-dimethylamino propyl)-N'-ethyl carbodiimide hydrochloride (EDC) (191.70 g/mol) solution was prepared with incomplete PBS (no Ca and Na ions). The CS, EDC, and NHS solutions were then combined in a 7:1.5:1.5 ratio (v/v) and thoroughly mixed on a stir plate. Following a 10 minute incubation in the 37°C oven, the solution was transferred to a beaker so that the total volume forms a thin layer that just covers the bottom. Immediately after the beaker was flash frozen in liquid nitrogen, an excess of previously chilled 95% ethanol was added. The mixture was allowed to stir for 30 minutes for the CS-NHS to precipitate. While waiting, the Buchnur funnel was prepared with two layers of filter paper (Whatman) and placed on top of the Bucher flask with a

rubber seal, which was connected to the vacuum. The CS-NHS product was removed from the beaker, transferred to the filter paper and tapped dry with a spatula prior to vacuum drying.

Individual spheroid delivery

Microdrilled bovine cartilage was removed from the tibia with a scalpel adhered to the bottom of a 35mm x 10mm Petri dish with an acrylate glue for subsequent procedures. The cartilage explant was sterilized by incubation in 95% ethyl alcohol for 1 hour, followed by two 30 min washes in complete PBS.

A 10% (w/v) 8-arm PEG amine solution and a 10% (w/v) CS-NHS solution were prepared in PBS and sterile filtered. The two solutions were then combined in a 1:1 ratio immediately before usage for spheroid placement in the cartilage defects.

Human MSC spheroids were formed by a forced aggregation method using agarose microwell inserts that were patterned from Aggrewells. A single cell MSC suspension (4.2 million cells) was added to the agarose microwell inserts and centrifuged (200 rcf, accel 0, decal 3) to aggregate cells within the microwells. After 24 hours, the fully formed 700-cell MSC spheroids were rinsed out of the microwells. Under a dissecting scope in a sterilely vented horizontal flow hood, individual hMSC spheroids were picked up with a 0.125mm diameter tungsten needle (Fine Science Tools, Foster City, CA) and placed into a microdefect in the cartilage explant. Immediately following placement, a drop of CS-NHS glue was laid over the MSC spheroid in the microdefect using the blunt end of the tungsten needle. The process was repeated until all defects have been filled. With a wide-bore pipette, 3mL of MSC growth media was then added to the

Petri dish to completely submerge the cartilage explant. The media was subsequently changed every other day for up to 7 days.

After 7 days in culture, the cartilage explant was incubated in the Live/Dead solution for 1 hour and washed in complete PBS for an additional hour. Fluorescence imaging of the explants was performed on the confocal microscope (Zeiss LSM 700, Oberkochen, Germany). For histology, the day 7 cartilage explant was fixed in 10% formalin for 1 hour by incubation. The explant was then washed in complete PBS for another hour before embedding in Histogel. A thin layer of histogel was first added to the bottom of a 10x10x5mm cryomold before placement of the cartilage explant and additional volume of histogel to ensure that the explant remains suspended while the histogel solidifies overnight. The histogel-embedded explant was then infiltrated in sucrose:OCT solutions of varying ratios using the standard protocol overnight under vacuum. The explant was transferred from well to well during the infiltration carefully so that the histogel remained intact. The infiltrated sample was then embedded in OCT for cryosectioning at 10μm thickness and stained with H&E. To visualize the spheroids in the explant, the aggregates were dipped in a Fast Green stain using the tungsten needle and rinsed off with PBS before placement in individual defects.

Results

A precise pattern of defects in the cartilage explant was achieved with microdrilling (Fig. A11A, arrows). The stereotaxic instrument allowed accurate control over the depth of each defect and the spacing between defects. Individual MSC spheroids could be placed in each defect with a coating of the CS-NHS glue for cartilage explant culture (Fig. A11B). After 7 days, histology and confocal microscopy confirmed the

presence of spheroids in the defects (Fig. A11C), which indicates that the shear forces from the flow of the media did not displace the spheroids. In addition, the MSC spheroids retained viability after one week in the cartilage explant culture as shown by the Live/Dead staining (Fig. A11D). The results suggest that the CS-NHS glue did not adversely affect diffusional transport of nutrients or other biomolecules to and from the MSC spheroids within the cartilage defects. Long term culture of spheroids in the bovine cartilage explants and more thorough characterization of the MSC phenotype after culture should be investigated in future studies.

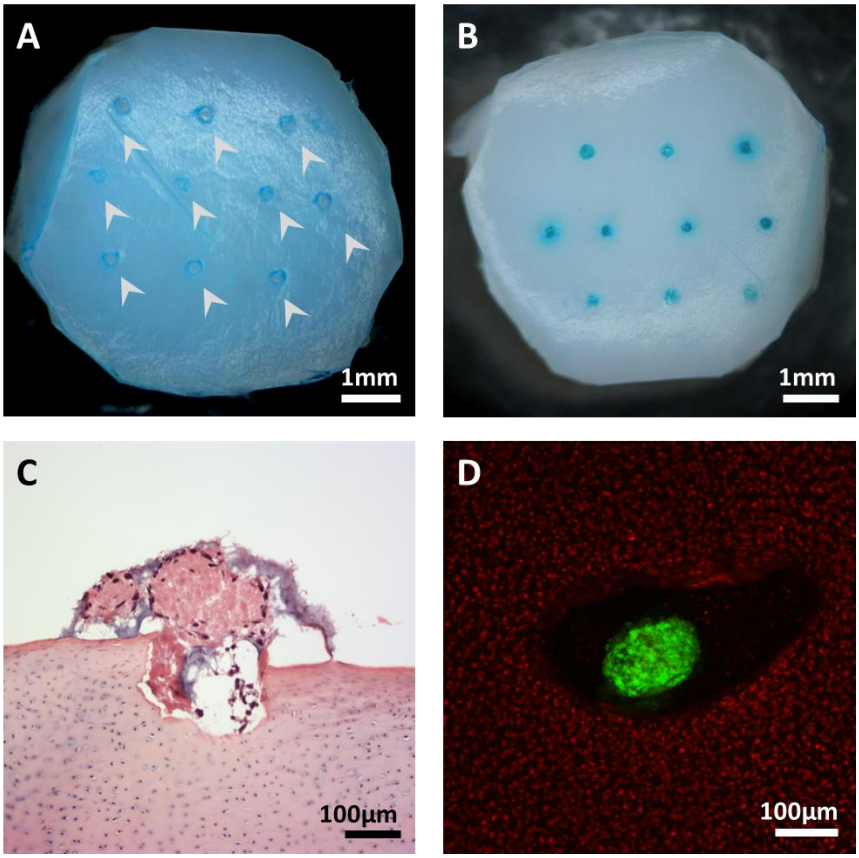

Figure A11. Visualization of MSC spheroid in cartilage microdefects. Alcian Blue staining of bovine cartilage demonstrated a distinct pattern of microdefects (A). MSC spheroids stained with Fast Green were individually placed in the cartilage microdefects (B). MSC spheroids remain in cartilage microdefects after 7 day in culture as shown by H&E staining (C). After 7 days in culture, MSC spheroids in cartilage microdefects remain viable (D). Scale bar = 1mm (A, B), scale bar = 100µm (C, D), n=3.

APPENDIX B

LABORATORY PROTOCOLS

CSMA Microparticle Preparation

CSMA Microparticle Formation

1) Remove chondroitin sulfate methacrylate (CSMA) from -20°C and allow to warm up to room temperature for 30 minutes on ice
2) Place 60 mL of corn oil in the 4°C refrigerator
3) Make APS solution in 1.5 mL tube: 34.2 mg APS in 500 µL PBS
4) Make TEMED solution in 1.5 mL tube: 22.5 µL in 500 µL PBS
5) Make sure everything is on ice to prevent crosslinking
6) Weigh out 55.6 mg CSMA in a scintillation vial and add 440uL of PBS
7) Homogenize corn oil at 3900 rpm for 5 minutes
8) Add 30 uL of APS and 30 uL of TEMED to the CSMA solution, mix, and add solution dropwise to corn oil (** Do NOT mix APS and TEMED together before adding to the CSMA solution**)
9) Homogenize emulsion for 5 minutes
10) Place corn oil mixture on a hot plate (set to 100°C) with the largest stir bar that will fit in the container (to keep particles moving so as not to crosslink with one another) and a thermometer (to monitor temperature - let it go up to 50-60°C).
11) Allow mixture to crosslink for 30 minutes with nitrogen purging
12) Set centrifuge temperature to 4°C

13) Separate mixture into two 50 mL conical tubes and centrifuge at a minimum of 1500 rpm for 5 minutes at 4°C
14) Remove oil from microparticles and resuspend pellet in ddH2O and transfer to 1.5 mL tube
15) Wash 3 times to remove oil
16) Store at 4°C for immediate use
17) For long term storage, remove all ddH2O and place in freezer for 10-20 min until frozen
18) Cover 1.5mL tubes with punctured aluminum foil and place in lyophilizer tube
19) Lyophilize until microparticles are dry (minimum overnight)
20) Remove lyophilized microparticles and store at -20°C

CSMA Microparticle Sterilization (before lyophilization)

1) Prior to lyophilization (step 17), add 1mL of 90% ethanol to the microparticles for 1 hour at 4°C on the rotary
2) Wash microparticles 3 times to remove ethanol
3) Remove all ethanol and place in freezer for 10-20 min until frozen
4) Cover 1.5mL tubes with punctured aluminum foil and place in lyophilizer tube
5) Lyophilize until microparticles are dry (minimum overnight)
6) Remove lyophilized sterile microparticles and store at -20°C

CSMA Microparticle Growth Factor Loading (after lyophilization)

1) Add growth factor dropwise to lyophilized microparticles at desired concentration (exp: 100ng TGF-β1 per mg of CSMA microparticles)
2) Incubate microparticles in growth factor solution overnight at 4°C on rotary

3) Remove supernatant and re-suspend in appropriate buffer (exp: media, PBS) for cell culture or release study

CSMA Microparticle Growth Factor Release

1) Loading concentration (from cell study): 100ng TGF-β1/1mg CSMA MP
2) 2mg CSMA MP/tube
3) 200ng TGF-β1/tube
4) Loading control: no MP + 200ng TGF-β1/tube (n=3)
    a. A no MP control has been previously done for growth factor loading
    b. Will be used to determine amounts of TGF-β not available for loading due to adsorption to the tube
5) Small volume (~50µL) loading
6) 18 hour overnight loading at 4°C
7) Time points: 3 hrs, 1, 3, 6, 9, 12, 15 days
    a. 3 hrs: burst release – unsequestered growth factors
8) Temperature: 37°C
9) Remove PBS at each time point and replenish with same volume (1mL)
10) Measure with ELISA (31pg/mL lowest sensitivity)

MSC Spheroid Formation

Materials

-3% w/v agarose solution
-glass jar
-AggreWell wafers
-70%EtOh
-Petri dish (100mm)
-tweezers (PDMS) or spatulas (agarose)
-MSCs and media
-6-well or 24-well plates
-Pipettor/pipettes
-Wide-bore pipette tips (1000uL)
-15mL centrifuge tubes
-1.7mL eppendorf tube (microcentrifuge tube)
-Regular pipette tips

Equipment

-Autoclave
-Microwave
-Centrifuge
-Plate holders for centrifuge
-LabRoller rotator (or any mini centrifuge tube rotisserie rotator)
-Rotary shaker
-Incubator

Methods

Making AggreWell Inserts with agarose:

1) Make a 3% (w/v) agarose solution, store in a glass jar at room temperature.
2) Autoclave using liquid cycle.
3) Spray AggreWell wafer with ethanol and wipe down to get off any particulates. Place in cell culture hoods under UV for at least 10 minutes.
4) If agarose solution is solid, heat up in microwave.
    a. Unscrew cap to loosen
    b. Heat in 1-2minute intervals. Shake in between heating.
    c. Note: Glass jar will get HOT, wear autoclave gloves.
5) Let jar cool and bring into hood.
6) Use pipette to transfer 3mL to each wafer insert. Use pipette tip to spread and cover whole area of insert.
7) Also use pipette to remove any bubbles or excess so that insert is not overfilled.

8) Let agarose solidify, will take 3-4 minutes.
9) Use flat and thin spatula to cut edge and scope out mold.
10) Transfer to 6-well plate. Use back of spatula (if it is rounded or flat) to push mold to the bottom of the mold.
11) If storing agarose molds overnight, add 2mL PBS to well with molds and store at room temperature.

Making Spheroids through UHTP/AggreWell method:

1) Prep cells for spheroids (trypsin, resuspension, counting).
2) Add media to the large (6-well) inserts or small (24-well) inserts so that the total volume after adding cells will be 3 mL for the large inserts or 1 mL for the small inserts.
3) Spin at 3000g for 5 minutes. (Accel/Decel: 9)
4) Add appropriate volume of cell solution and let settle for 5 minutes.
    a. For 1000-cell spheroid, add 6 x 10^6 cells to large (6-well) inserts (~6000 spheroids)
    b. Make 500-cell MSC spheroids for anti-inflammatory assay
    c. If adding particles, add the particles to cell solution and mix, then transfer cells/microparticle solution to wells. Microparticle:cell ratio depends on microparticle composition and spheroid size.
5) Spin at 200 g for 5 minutes. (Acceleration: 0, Deceleration: 3)
6) Place plate in incubator where it will not be disturbed (try not to bump!) for 1 day.
7) After 16-18 hours, use a wide-bore pipette tip to “pop out” the spheroids by gently pipetting up and down with media gently all over the insert, then transfer

volume to a 15mL centrifuge tube. Add fresh media into well plates and repeat pipetting “pop out” as necessary until all EBs/spheroids are removed (2-3x). Minimize bubble formation.

8) Check inserts under microscope for any leftover spheroids.
    a. For PDMS inserts, do not let cells incubate for longer than 18hrs- spheroids will start to adhere to PDMS, making it difficult to “pop out”.
9) Let the spheroids settle (~5min) in centrifuge tube, then remove all but the bottom 1 mL of volume. Do not aspirate, just use pipettor to take off supernatant media.
    a. If settling takes a long time, place centrifuge tube in incubator and wait ~10 minutes.
10) Add 9 mL of media to centrifuge tube and transfer to non-tissue culture treated 100mm petri dishes.
    a. Large inserts are typically split into 3 plates, while small inserts are enough for one plate
11) To change media, transfer spheroid suspension to 15mL centrifuge tube (make sure no spheroids left on plate). Let spheroids settle in tube, and remove 9mL of spent media, replace with 9mL fresh media. Transfer solution back to petri dish.

MSC Spheroid Alginate Encapsulation

Background

- Alginate encapsulation of MSC spheroids minimizes agglomeration and loss of aggregates over extended culture periods (up to 21+ days)
- Protocol below is written specifically for MSC spheroids, but can be applied to other cell types

Materials

- 1.5% sodium alginate in ddH_20 (sterile filtered)
- 100mM calcium chloride (sterile filtered)
- 55mM sodium citrate (sterile filtered)
- 10U/mL alginate lyase (non-sterile)
- #4 Whatman filter paper 125mm (trimmed to 75mm diameter, autoclaved)
- Forceps (autoclaved)
- Low attachment plates

Protocols

Alginate Encapsulation (after formation of spheroids in insert):

1. Pellet MSC spheroids and aspirate media supernatant
2. Wash spheroids with complete PBS
3. Add alginate to the pellet and mix for a uniform solution
    - ~5mL of alginate can be used to form one gel depending on desirable thickness
4. Prepare a petri dish of $CaCl_2$ solution

5. Using a pair of forceps, fully soak the filter paper in the $CaCl_2$
6. Carefully place the filter paper over the alginate
    - The filter paper will draw the alginate across the entire plate
7. Add 2mL of $CaCl_2$ on top of the filter paper
8. Allow alginate to crosslink for 10 minutes
9. Remove the filter paper with the forceps
10. Add 9mL of media to the plate

Alginate Dissociation (for collecting samples):

1. Aspirate all of the media
2. Wash alginate gel with incomplete PBS (at least two times) until it is no longer pink
3. Add 10mL of sodium citrate per plate
4. Incubate on the rotary at 37°C for 30 minutes
5. Transfer the sodium citrate-spheroid mixtures to conical tubes
6. Pipette up and down to ensure all of the alginate has dissociated
7. Add more sodium citrate if necessary to dissociate any alginate remnants
8. Allow spheroids to pellet and aspirate the sodium citrate
9. Wash spheroids with complete PBS (at least two times)
10. Add 300µL of alginate lyase to the pellet
11. Incubate at 37°C for 20 minutes
12. Remove the alginate lyase and collect samples accordingly

Immunohistochemistry

General Materials

Fixative (Acetone, formalin, formaldehyde)

Block serum (1.5% in PBS)

1°Ab (in 1.5% serum)

2°Ab (in 1.5% serum)

Nuclear counterstain (Hoechst 1:100 in ddH_2O)

Image-iT FX Signal Enhancer (Life Technologies, I36933)

Primary Antibodies

1° Antibody	Order Info	Isoform	Dilution	Deglycosylate	Blocking
Aggrecan	Abcam (ab3778)	IgG	1:20	Y	Image-iT
Collagen I	Abcam (ab90935)	IgG	1:60	N	Image-iT
Collagen II	Abcam (ab3092)	IgG	1:20	N	Image-iT
Collagen X	Sigma (C7974)	IgM	1:20	Y	Serum
IgG Isotype	Abcam (ab91353)	IgG	1:10	N	Image-iT
IgM Isotype	Abcam (ab18401)	IgM	1:50	N	Serum

Deglycosylation

Activation buffer (50mM Tris, 60mM sodium acetate, 0.02% BSA, pH 8.0)

Activate chondroitinase ABC in the activation buffer

Dilute 1 U/mL chondroitinase 3:4 with 4X activating buffer

(e.g. 0.75mL chondroitinase and 0.25mL buffer)

Antigen Retrieval

TE-$CaCl_2$ buffer (50mM Tris Base, 1mM EDTA, 5mM $CaCl_2$, 0.5% Triton X-100, pH 8.0)

- Tris Base (6.10g)
- EDTA (0.37g)
- CaCl2 (0.56g)
- Triton X-100 (5mL)
- Distilled Water (1000mL)
- Store at room temperature

Proteinase K stock solution (20X, 400µg/mL)

- Proteinase K (30 U/mg) (8mg)
- TE-$CaCl_2$ buffer (10mL)
- Glycerol (10mL)
- Add proteinase K to TE-$CaCl_2$ buffer until dissolved
- Add glycerol and mix well
- Aliquot and store at -20°C for 2-3 years

Proteinase K working solution (1X, 20µg/mL)

- Proteinase K stock solution (1mL)
- TE-$CaCl_2$ buffer (19mL)
- Mix well
- Stable at 4°C for 6 months

Frozen Sections

1) Incubate in water for 5 min to remove OCT
2) For unfixed sections:
    a. Fix in acetone (NBF, paraformaldehyde, methanol) for 5 min
    b. Wash 2X in PBS for 5 min
3) For fixed sections:
    a. Incubate in Proteinase K solution for 10 min at 37°C
    b. Wash 2X in PBS for 5 min
4) For Aggrecan and Collagen X antibodies:

a. Deglycosylate in 0.75U/mL chondroitinase ABC (30µL) for 1.5 hours at 37°C
b. Wash 2X in PBS for 5 min

5) Block with 1.5% serum from species of secondary Ab in PBS for 1 hour
6) Incubate in 1°Ab (in 1.5% serum) at RT for 1 hour or 4°C overnight
7) Wash 3X in PBS for 5min
8) Incubate in 2°Ab (1:200) (in 1.5% serum) at RT for 1 hour
9) Wash 3X in PBS for 5 min
10) Incubate in nuclear counterstain (Hoechst) for 5 min
11) Wash 2X in PBS for 5min
12) Wash in water for 5min
13) Coverslip with mounting media and store in 4°C overnight

IHC Worksheet

Step	Solution	Time	Temp	Concen	Volume
1	Water	5 min	RT		
2	Fixative	20 min	RT		
3	PBS	5 min	RT		
4	PBS	5 min	RT		
5	Proteinase K	10min	37°C		100µL x _____=_____ µL
6	PBS	5 min	RT		
7	PBS	5 min	RT		
8	Chondroitinase ABC	1.5 hour	37°C		30µL x _____=_____ µL
9	PBS	5 min	RT		
10	PBS	5 min	RT		
11	Block (serum or Image-iT)	30 min	RT		
*	PBS (Image-iT)	5 min			
*	PBS (Image-iT)	5 min			
12	1°Antibody/Isotype	Overnight	4°C	1:20	100µL x _____=_____ µL
13	PBS	5 min	RT		
14	PBS	5 min	RT		
15	PBS	5 min	RT		
16	2°Antibody	30 min	RT	1:200	100µL x _____=_____ µL
17	PBS	5 min	RT		
18	PBS	5 min	RT		
19	PBS	5 min	RT		
20	Nuclear Stain	5 min	RT	1:100	100µL x _____=_____µL
21	PBS	5 min	RT		
22	PBS	5 min	RT		
23	Water	5 min	RT		
24	Coverslip	5 min	4°C		

CS-NHS Conjugation (adapted from Torri Rinker)

Reagents

- Chondrotin Sulfate C (CSC): 463.369 g/mol
- N-hydroxysuccinimide (NHS): 115.087 g/mol
- N-(3-dimethylamino propyl)-N'-ethyl carbodiimide hydrochloride (EDC): 191.70 g/mol
- PBS (without Ca and Na)

Supplies

- aluminum foil, needle
- vortex
- Buchner flask
- Buchnur funnel
- 2 filter papers
- Tubing
- high vacuum
- ethanol (EtOH)
- scintillation vial

CS-NHS Conjugation Procedure

1) Store 95% EtOH in -20°C

2) Make the following solutions in PBS and mix well:

    a. 10% (w/v) CS-C

    b. 25% (w/v) NHS

    c. 67% (w/v) EDC

3) Combine CS, EDC, and NHS in a 7:1.5:1.5 ratio (v/v)

    a. Volume CS:

    b. Volume NHS:

    c. Volume EDC:

4) Mix on stir plate in hood

5) Place in the 37°C oven for 10 minutes.

6) Transfer to a beaker so that the total volume just covers the bottom, making a thin layer.

Flash freeze in liquid nitrogen.

7) Immediately add an excess of -20°C 95% EtOH to the beaker (_____ mL)

8) Wait 30 minutes for CS-NHS to precipitate while stirring.

9) Place two filter papers in the Buchnur funnel and place the funnel on top of the Bucher flask with a rubber seal. Hook flask to vacuum.

10) Transfer the product from the beaker to the filter paper. Rinse the beaker with EtOH (_____ mL). Keep the liquid portion for assaying purposes.

11) Use a spatula to split up the product and get it as dry as possible. Then, vacuum dry.

CS-NHS Glue Procedure

1) Dissolve CS-NHS in PBS (10% w/v) and the 8 arm PEG in PBS (10% w/v) first

2) For a total of 100uL, weigh out10mg of CS-NHS and add it to 100uL of PBS

3) Make about 200uL extra for sterile filtering.

4) Combine the CS-NHS and PEG in a 1:1 ratio.

5) The glue needs to be used right away and cannot be store.

REFERENCES

1. Murphy, L., et al., *Lifetime risk of symptomatic knee osteoarthritis.* Arthritis Rheum, 2008. **59**(9): p. 1207-13.
2. Murphy, L. and C.G. Helmick, *The impact of osteoarthritis in the United States: a population-health perspective: A population-based review of the fourth most common cause of hospitalization in U.S. adults.* Orthop Nurs, 2012. **31**(2): p. 85-91.
3. Goldring, M.B. and S.R. Goldring, *Articular cartilage and subchondral bone in the pathogenesis of osteoarthritis.* Ann N Y Acad Sci, 2010. **1192**: p. 230-7.
4. Loeser, R.F., et al., *Osteoarthritis: a disease of the joint as an organ.* Arthritis Rheum, 2012. **64**(6): p. 1697-707.
5. Temenoff, J.S. and A.G. Mikos, *Review: tissue engineering for regeneration of articular cartilage.* Biomaterials, 2000. **21**(5): p. 431-40.
6. Reboul, P., et al., *The new collagenase, collagenase-3, is expressed and synthesized by human chondrocytes but not by synoviocytes. A role in osteoarthritis.* Journal of Clinical Investigation, 1996. **97**(9): p. 2011.
7. Goldring, M.B., *The role of the chondrocyte in osteoarthritis.* Arthritis & Rheumatism, 2000. **43**(9): p. 1916-1926.
8. Goldring, M.B., *Chondrogenesis, chondrocytes differentiation, and articular cartilage metabolism in health and osteoarthritis* Ther Adv Musculoskel Dis, 2012. **4**(4): p. 269-85.
9. Sellam, J. and F. Berenbaum, *The role of synovitis in pathophysiology and clinical symptoms of osteoarthritis.* Nature Reviews Rheumatology, 2010. **6**(11): p. 625-635.
10. Nesic, D., et al., *Cartilage tissue engineering for degenerative joint disease.* Adv Drug Deliv Rev, 2006. **58**(2): p. 300-22.
11. Muir, H., *The chondrocyte, architect of cartilage. Biomechanics, structure, function and molecular biology of cartilage matrix macromolecules.* BioEssays, 1995. **17**(12): p. 1039-48.
12. Roughley, P.J. and E.R. Lee, *Cartilage proteoglycans: structure and potential functions.* Microscopy Research and Technique, 1994. **28**(5): p. 385-97.
13. Mahmoudifar, N. and P.M. Doran, *Chondrogenesis and cartilage tissue engineering: the longer road to technology development.* Trends Biotechnol, 2012. **30**(3): p. 166-76.
14. Jin, R., et al., *Chondrogenesis in injectable enzymatically crosslinked heparin/dextran hydrogels.* Journal of Controlled Release, 2011. **152**(1): p. 186-195.
15. Poole, A.R., et al., *Composition and Structure of Articular Cartilage: A Template for Tissue Repair.* Clinical Orthopaedics and Related Research, 2001. **391**: p. S22-36.
16. Kjellen, L. and U. Lindahl, *Proteoglycans: Structures and Interactions.* Annu Rev Biochem, 1991. **60**: p. 443-75.
17. Knudson, C.B. and W. Knudson, *Cartilage proteoglycans.* Semin Cell Dev Biol, 2001. **12**(2): p. 69-78.

18. Miller, T., et al., *Molecular engineering of glycosaminoglycan chemistry for biomolecule delivery.* Acta Biomater, 2013.
19. Bayliss, M.T., et al., *Sulfation of Chondroitin Sulfate in Human Articular Cartilage: The Effect of Age, Topographical Position, and Zone of Cartilage on Tisse Composition.* Journal of Biological Chemistry, 1999. **274**(22): p. 15892-15900.
20. Olsen, B.R., A.M. Reginato, and W. Wang, *Bone development.* Annual review of cell and developmental biology, 2000. **16**(1): p. 191-220.
21. Oberlender, S.A. and R.S. Tuan, *Spatiotemporal profile of N-cadherin expression in the developing limb mesenchyme.* Cell Communication and Adhesion, 1994. **2**(6): p. 521-537.
22. Oberlender, S.A. and R.S. Tuan, *Expression and functional involvement of N-cadherin in embryonic limb chondrogenesis.* Development, 1994. **120**: p. 177-87.
23. Tavella, S., et al., *N-CAM and N-Cadherin Expression during In Vitro Chondrogenesis.* Experimental cell research, 1994. **215**(2): p. 354-362.
24. Hidaka, C. and M.B. Goldring, *Regulatory mechanicsms of chondrogenesis and implications for understanding articular cartilage homeostasis.* Current Rheumatology Reviews, 2008. **4**: p. 1-12.
25. Yoon, B.S., et al., *Bmpr1a and Bmpr1b have overlapping functions and are essential for chondrogenesis in vivo.* Proceedings of the National Academy of Sciences of the United States of America, 2005. **102**(14): p. 5062-5067.
26. Pitsillides, A.A. and F. Beier, *Cartilage biology in osteoarthritis--lessons from developmental biology.* Nat Rev Rheumatol, 2011. **7**(11): p. 654-63.
27. Goldring, M.B., K. Tsuchimochi, and K. Ijiri, *The control of chondrogenesis.* J Cell Biochem, 2006. **97**(1): p. 33-44.
28. Ferguson, C.M., et al., *Common molecular pathways in skeletal morphogenesis and repair.* Annals of the New York Academy of Sciences, 1998. **857**(1): p. 33-42.
29. Watanabe, H., Y. Yamada, and K. Kimata, *Roles of aggrecan, a large chondroitin sulfate proteoglycan, in cartilage struction and function.* Journal of Biochemistry, 1998. **124**: p. 687-93.
30. Domowicz, M.S., et al., *Aggrecan modulation of growth plate morphogenesis.* Dev Biol, 2009. **329**(2): p. 242-57.
31. Kimata, K., et al., *A large chondroitin sulfate proteoglycan synthesized before chondrogenesis in the limb bud of chick embryo.* Journal of Biological Chemistry, 1986. **261**(29): p. 13517-25.
32. Choocheep, K., et al., *Versican facilitates chondrocyte differentiation and regulates joint morphogenesis.* J Biol Chem, 2010. **285**(27): p. 21114-25.
33. Dobratz, E.J., et al., *Injectable cartilage using alginate and human chondrocyte.* Archives of Facial Plastic Surgery, 2009. **11**(1): p. 40-47.
34. Schrobback, K., et al., *Adult human articular chondrocytes in a microcarrier-based culture system: expansion and redifferentiation.* J Orthop Res, 2011. **29**(4): p. 539-46.
35. Kim, M., et al., *The use of de-differentiated chondrocytes delivered by a heparin-based hydrogel to regenerate cartilage in partial-thickness defects.* Biomaterials, 2011. **32**(31): p. 7883-96.

36. Paige, K.T., et al., *De novo cartilage generation using calcium alginate-chondrocyte constructs.* Plastic and Reconstructive Surgery, 1996. **97**(1): p. 168-78.
37. Chung, C. and J.A. Burdick, *Engineering cartilage tissue.* Adv Drug Deliv Rev, 2008. **60**(2): p. 243-62.
38. Darling, E.M. and K.A. Athanasiou, *Rapid phenotypic changes in passaged articular chondrocyte subpopulations.* Journal of Orthopaedic Research, 2005. **23**(2): p. 425-432.
39. Winter, A., et al., *Cartilage-like gene expression in differentiated human stem cell spheroids: a comparison of bone marrow-derived and adipose tissue-derived stromal cells.* Arthritis Rheum, 2003. **48**(2): p. 418-29.
40. Im, G.I., Y.W. Shin, and K.B. Lee, *Do adipose tissue-derived mesenchymal stem cells have the same osteogenic and chondrogenic potential as bone marrow-derived cells?* Osteoarthritis Cartilage, 2005. **13**(10): p. 845-53.
41. Song, L., D. Baksh, and R.S. Tuan, *Mesenchymal stem cell-based cartilage tissue engineering: cells, scaffold and biology.* Cytotherapy, 2004. **6**(6): p. 596-601.
42. Engler, A.J., et al., *Matrix elasticity directs stem cell lineage specification.* Cell, 2006. **126**(4): p. 677-89.
43. Kshitiz, et al., *Control of stem cell fate and function by engineering physical microenvironments.* Integrative Biology, 2012. **4**(9): p. 1008.
44. Freyria, A.M. and F. Mallein-Gerin, *Chondrocytes or adult stem cells for cartilage repair: the indisputable role of growth factors.* Injury, 2012. **43**(3): p. 259-65.
45. Mackay, A.M., et al., *Chondrogenic differentiation of cultured h mesenchymal stem cells from marrow.* Tissue Eng 1998. **4**(4): p. 415-28.
46. Sekiya, I., et al., *Comparison of effect of BMP-2,-4, and-6 on in vitro cartilage formation of human adult stem cells from bone marrow stroma.* Cell and tissue research, 2005. **320**(2): p. 269-276.
47. Indrawattana, N., et al., *Growth factor combination for chondrogenic induction from human mesenchymal stem cell.* Biochem Biophys Res Commun, 2004. **320**(3): p. 914-9.
48. Johnstone, B., et al., *In Vitro Chondrogenesis of Bone Marrow-Derived Mesenchymal Progenitor Cells.* Experimental cell research, 1998. **238**(1): p. 265-272.
49. Hall, B.K. and T. Miyake, *Divide, accumulate, differentiate: cell condensation in skeletal development revisited.* International Journal of Developmental Biology, 1995. **39**: p. 881-894.
50. Quintana, L., N.I. zur Nieden, and C.E. Semino, *Morphogenetic and regulatory mechanisms during developmental chondrogenesis: new paradigms for cartilage tissue engineering.* Tissue Engineering Part B: Reviews, 2008. **15**(1): p. 29-41.
51. Chimal-Monroy, J. and L.D. De Leon, *Expression of N-cadherin, N-CAM, fibronectin and tenascin is stimulated by TGF-B1, B2, B3, B5 during the formation of precartilage condensations.* International Journal of Developmental Biology, 1999. **43**: p. 59-67.

52. Richardson, S.M., et al., *Mesenchymal stem cells in regenerative medicine: opportunities and challenges for articular cartilage and intervertebral disc tissue engineering.* J Cell Physiol, 2010. **222**(1): p. 23-32.
53. Farrell, E., et al., *Chondrogenic priming of human bone marrow stromal cells a better route to bone repair.* Tissue Eng Part C Methods, 2009. **15**(2): p. 285-95.
54. Pelttari, K., et al., *Premature induction of hypertrophy during in vitro chondrogenesis of human mesenchymal stem cells correlates with calcification and vascular invasion after ectopic transplantation in SCID mice.* Arthritis Rheum, 2006. **54**(10): p. 3254-66.
55. Duval, E., et al., *Molecular mechanism of hypoxia-induced chondrogenesis and its application in in vivo cartilage tissue engineering.* Biomaterials, 2012. **33**(26): p. 6042-51.
56. Foldager, C.B., et al., *Combined 3D and hypoxic culture improves cartilage-specific gene expression in human chondrocytes.* Acta Orthop, 2011. **82**(2): p. 234-40.
57. Gawlitta, D., et al., *Hypoxia impedes hypertrophic chondrogenesis of human multipotent stromal cells.* Tissue Eng Part A, 2012. **18**(19-20): p. 1957-66.
58. Sheehy, E.J., C.T. Buckley, and D.J. Kelly, *Oxygen tension regulates the osteogenic, chondrogenic and endochondral phenotype of bone marrow derived mesenchymal stem cells.* Biochem Biophys Res Commun, 2012. **417**(1): p. 305-10.
59. Feinberg, R.N., C.H. Latker, and D.C. Beebe, *Localized vascular regression during limb morphogenesis in the chicken embryo. I. Spatial and temporal changes in the vascular pattern.* The Anatomical Record, 1986. **214**(4): p. 405-409.
60. Hallmann, R., et al., *Regression of blood vessels precedes cartilage differentiation during chick limb development.* Differentiation, 1987. **34**(2): p. 98-105.
61. Schipani, E., *Hypoxia and HIF-1 alpha in chondrogenesis.* Semin Cell Dev Biol, 2005. **16**(4-5): p. 539-46.
62. Park, J.H., et al., *Hypoxia decreases RUNX2/Cbfa1 expression in human osteoblast-like cells.* Molecular and Cellular Endocrinology, 2002. **192**: p. 197-203.
63. Hirao, M., et al., *Oxygen tension regulates chondrocyte differentiation and function during endochondral ossification.* J Biol Chem, 2006. **281**(41): p. 31079-92.
64. Amarilio, R., et al., *HIF1alpha regulation of Sox9 is necessary to maintain differentiation of hypoxic prechondrogenic cells during early skeletogenesis.* Development, 2007. **134**(21): p. 3917-28.
65. Robins, J.C., et al., *Hypoxia induces chondrocyte-specific gene expression in mesenchymal cells in association with transcriptional activation of Sox9.* Bone, 2005. **37**(3): p. 313-22.
66. Murphy, C.L. and J.M. Polak, *Control of human articular chondrocyte differentiation by reduced oxygen tension.* J Cell Physiol, 2004. **199**(3): p. 451-9.
67. Krinner, A., et al., *Impact of oxygen environment on mesenchymal stem cell expansion and chondrogenic differentiation.* Cell Prolif, 2009. **42**(4): p. 471-84.

68. Zscharnack, M., et al., *Low oxygen expansion improves subsequent chondrogenesis of ovine bone-marrow-derived mesenchymal stem cells in collagen type I hydrogel.* Cells Tissues Organs, 2009. **190**(2): p. 81-93.
69. Meretoja, V.V., et al., *The effect of hypoxia on the chondrogenic differentiation of co-cultured articular chondrocytes and mesenchymal stem cells in scaffolds.* Biomaterials, 2013. **34**(17): p. 4266-73.
70. Markway, B.D., et al., *Enhanced chondrogenic differentiation of human bone marrow-derived mesenchymal stem cells in low oxygen environment micropellet cultures.* Cell Transplant, 2010. **19**(1): p. 29-42.
71. Carpenedo, R.L., et al., *Homogeneous and organized differentiation within embryoid bodies induced by microsphere-mediated delivery of small molecules.* Biomaterials, 2009. **30**(13): p. 2507-15.
72. Pampaloni, F., E.G. Reynaud, and E.H. Stelzer, *The third dimension bridges the gap between cell culture and live tissue.* Nature reviews Molecular cell biology, 2007. **8**(10): p. 839-845.
73. Lin, R.Z. and H.Y. Chang, *Recent advances in three-dimensional multicellular spheroid culture for biomedical research.* Biotechnol J, 2008. **3**(9-10): p. 1172-84.
74. Frith, J.E., B. Thomson, and P.G. Genever, *Dynamic 3D culture methods enhance MSC properties and increase therapeutic potential.* Tissue Eng Part C Methods, 2010. **16**(4): p. 735-49.
75. Yuhas, J.M., et al., *A simplified method for production and growth of multicellular tumor spheroids.* Cancer Research, 1977. **37**: p. 3639-43.
76. Liu, J., et al., *Functional three-dimensional HepG2 aggregate cultures generated from an ultrasound trap: comparison with HepG2 spheroids.* J Cell Biochem, 2007. **102**(5): p. 1180-9.
77. Ho, V.H., et al., *Generation and manipulation of magnetic multicellular spheroids.* Biomaterials, 2010. **31**(11): p. 3095-102.
78. Li, A.P., S.M. Colburn, and D.J. Beck, *A simplified method for the culturing of primary adult rat and human hepatocytes as multicellular spheroids.* In Vitro Cell Developmental Biology, 1992. **28A**: p. 673-77.
79. Kelm, J.M. and M. Fussenegger, *Microscale tissue engineering using gravity-enforced cell assembly.* Trends Biotechnol, 2004. **22**(4): p. 195-202.
80. Baraniak, P.R. and T.C. McDevitt, *Scaffold-free culture of mesenchymal stem cell spheroids in suspension preserves multilineage potential.* Cell Tissue Res, 2012. **347**(3): p. 701-11.
81. Kelm, J.M., et al., *Method for generation of homogeneous multicellular tumor spheroids applicable to a wide variety of cell types.* Biotechnol Bioeng, 2003. **83**(2): p. 173-80.
82. Souza, G.R., et al., *Three-dimensional tissue culture based on magnetic cell levitation.* Nature nanotechnology, 2010. **5**(4): p. 291-296.
83. Ungrin, M.D., et al., *Reproducible, Ultra High-Throughput Formation of Multicellular Organization from Single Cell Suspension-Derived Human Embryonic Stem Cell Aggregates.* PLoS One, 2008. **3**(2): p. 1-12.
84. Bocchi, M., et al., *Inverted open microwells for cell trapping, cell aggregate formation and parallel recovery of live cells.* Lab Chip, 2012. **12**(17): p. 3168-76.

85. Stevens, K.R., et al., *InVERT molding for scalable control of tissue microarchitecture.* Nat Commun, 2013. **4**: p. 1847.
86. Napolitano, A.P., et al., *Dynamics of the self-assembly of complex cellular aggregates on micromolded nonadhesive hydrogels.* Tissue engineering, 2007. **13**(8): p. 2087-2094.
87. Khademhosseini, A., et al., *Co-culture of human embryonic stem cells with murine embryonic fibroblasts on microwell-patterned substrates.* Biomaterials, 2006. **27**(36): p. 5968-77.
88. Choi, Y.Y., et al., *Controlled-size embryoid body formation in concave microwell arrays.* Biomaterials, 2010. **31**(15): p. 4296-303.
89. Mohr, J.C., J.J. de Pablo, and S.P. Palecek, *3-D microwell culture of human embryonic stem cells.* Biomaterials, 2006. **27**(36): p. 6032-42.
90. Bratt-Leal, A.M., et al., *Incorporation of biomaterials in multicellular aggregates modulates pluripotent stem cell differentiation.* Biomaterials, 2011. **32**(1): p. 48-56.
91. Wang, W., et al., *3D spheroid culture system on micropatterned substrates for improved differentiation efficiency of multipotent mesenchymal stem cells.* Biomaterials, 2009. **30**(14): p. 2705-15.
92. Babur, B.K., et al., *The interplay between chondrocyte redifferentiation pellet size and oxygen concentration.* PLoS One, 2013. **8**(3): p. e58865.
93. Wang, C.C., et al., *Spherically symmetric mesenchymal stromal cell bodies inherent with endogenous extracellular matrices for cellular cardiomyoplasty.* Stem Cells, 2009. **27**(3): p. 724-32.
94. Bartosh, T.J., et al., *Aggregation of human mesenchymal stromal cells (MSCs) into 3D spheroids enhances their antiinflammatory properties.* Proc Natl Acad Sci U S A, 2010. **107**(31): p. 13724-29.
95. Ylostalo, J.H., et al., *Human mesenchymal stem/stromal cells cultured as spheroids are self-activated to produce prostaglandin E2 that directs stimulated macrophages into an anti-inflammatory phenotype.* Stem Cells, 2012. **30**(10): p. 2283-96.
96. Peppas, N.A., et al., *Hydrogels in Biology and Medicine: From Molecular Principles to Bionanotechnology.* Advanced Materials, 2006. **18**(11): p. 1345-1360.
97. Scott, R.A. and A. Panitch, *Glycosaminoglycans in biomedicine.* Wiley Interdisciplinary Reviews-Nanomedicine and Nanobiotechnology, 2013. **5**(4): p. 388-398.
98. Prokoph, S., et al., *Sustained delivery of SDF-1alpha from heparin-based hydrogels to attract circulating pro-angiogenic cells.* Biomaterials, 2012. **33**(19): p. 4792-800.
99. Kim, M., et al., *Heparin-based hydrogel as a matrix for encapsulation and cultivation of primary hepatocytes.* Biomaterials, 2010. **31**(13): p. 3596-603.
100. Nie, T., R.E. Akins, Jr., and K.L. Kiick, *Production of heparin-containing hydrogels for modulating cell responses.* Acta Biomater, 2009. **5**(3): p. 865-75.
101. Liang, Y. and K.L. Kiick, *Heparin-functionalized polymeric biomaterials in tissue engineering and drug delivery applications.* Acta Biomater, 2013.

102. Jin, R., et al., *Enzyme-mediated fast in situ formation of hydrogels from dextran-tyramine conjugates.* Biomaterials, 2007. **28**(18): p. 2791-800.
103. Lim, J.J. and J.S. Temenoff, *The effect of desulfation of chondroitin sulfate on interactions with positively charged growth factors and upregulation of cartilaginous markers in encapsulated MSCs.* Biomaterials, 2013. **34**(21): p. 5007-5018.
104. Varghese, S., et al., *Chondroitin sulfate based niches for chondrogenic differentiation of mesenchymal stem cells.* Matrix Biol, 2008. **27**(1): p. 12-21.
105. Guo, Y., et al., *Hydrogels of collagen/chondroitin sulfate/hyaluronan interpenetrating polymer network for cartilage tissue engineering.* J Mater Sci Mater Med, 2012. **23**(9): p. 2267-79.
106. Nguyen, L.H., et al., *Unique biomaterial compositions direct bone marrow stem cells into specific chondrocytic phenotypes corresponding to the various zones of articular cartilage.* Biomaterials, 2011. **32**(5): p. 1327-38.
107. Machado, C.B., et al., *3D chitosan-gelatin-chondroitin porous scaffold improves osteogenic differentiation of mesenchymal stem cells.* Biomed Mater, 2007. **2**(2): p. 124-31.
108. Simson, J.A., et al., *An adhesive bone marrow scaffold and bone morphogenetic-2 protein carrier for cartilage tissue engineering.* Biomacromolecules, 2013. **14**(3): p. 637-43.
109. Bryant, S.J., J.A. Arthur, and K.S. Anseth, *Incorporation of tissue-specific molecules alters chondrocyte metabolism and gene expression in photocrosslinked hydrogels.* Acta Biomater, 2005. **1**(2): p. 243-52.
110. Simson, J.A., et al., *Bonding and fusion of meniscus fibrocartilage using a novel chondroitin sulfate bone marrow tissue adhesive.* Tissue Eng Part A, 2013. **19**(15-16): p. 1843-51.
111. Wang, D.A., et al., *Multifunctional chondroitin sulphate for cartilage tissue-biomaterial integration.* Nat Mater, 2007. **6**(5): p. 385-92.
112. Strehin, I., et al., *A versatile pH sensitive chondroitin sulfate-PEG tissue adhesive and hydrogel.* Biomaterials, 2010. **31**(10): p. 2788-97.
113. Almond, A., *Hyaluronan.* Cellular and Molecular Life Sciences, 2007. **64**(13): p. 1591-1596.
114. Fakhari, A. and C. Berkland, *Applications and emerging trends of hyaluronic acid in tissue engineering, as a dermal filler and in osteoarthritis treatment.* Acta Biomater, 2013. **9**(7): p. 7081-92.
115. Davidenko, N., et al., *Collagen-hyaluronic acid scaffolds for adipose tissue engineering.* Acta Biomater, 2010. **6**(10): p. 3957-68.
116. Wang, W.H., et al., *Cross-linked Collagen-Chondroitin Sulfate-Hyaluronic Acid Imitating Extracellular Matrix as Scaffold for Dermal Tissue Engineering.* Tissue Engineering Part C-Methods, 2010. **16**(2): p. 269-279.
117. Matsiko, A., et al., *Addition of hyaluronic acid improves cellular infiltration and promotes early-stage chondrogenesis in a collagen-based scaffold for cartilage tissue engineering.* J Mech Behav Biomed Mater, 2012. **11**: p. 41-52.
118. Shah, D.N., S.M. Recktenwall-Work, and K.S. Anseth, *The effect of bioactive hydrogels on the secretion of extracellular matrix molecules by valvular interstitial cells.* Biomaterials, 2008. **29**(13): p. 2060-72.

119. Ifkovits, J.L., et al., *Injectable hydrogel properties influence infarct expansion and extent of postinfarction left ventricular remodeling in an ovine model.* Proc Natl Acad Sci U S A, 2010. **107**(25): p. 11507-12.
120. Hwang, N.S., et al., *Regulation of osteogenic and chondrogenic differentiation of mesenchymal stem cells in PEG-ECM hydrogels.* Cell Tissue Res, 2011. **344**(3): p. 499-509.
121. Kwon, J.S., et al., *Injectable in situ-forming hydrogel for cartilage tissue engineering.* Journal of Materials Chemistry B, 2013. **1**(26): p. 3314.
122. Lum, L. and J. Elisseeff, *Injectable hydrogels for cartilage tissue engineering*, in *Topics in Tissue Engineering*, N. Ashammakhi and P. Ferretti, Editors. 2003, University of Oulu. p. 1-25.
123. Temenoff, J.S. and A.G. Mikos, *Injectable biodegradable materials for orthopedic tissue engineering.* Biomaterials, 2000. **21**: p. 2405-12.
124. Amini, A.A. and L.S. Nair, *Injectable hydrogels for bone and cartilage repair.* Biomed Mater, 2012. **7**(2): p. 024105.
125. Stevens, M., *A rapid-curing alginate gel system: utility in periosteum-derived cartilage tissue engineering.* Biomaterials, 2004. **25**(5): p. 887-894.
126. Peretti, G.M., et al., *Review of injectable cartilage engineering using fibrin gel in mice and swine models.* Tissue engineering, 2006. **12**(5): p. 1151-1168.
127. Silverman, R.P., et al., *Injectable tissue-engineered cartilage using a fibrin glue polymer.* Plastic and Reconstructive Surgery, 1999. **103**(7): p. 1809-18.
128. Wennink, J., *Injectable hydrogels for articular cartilage tissue engineering.* 2013.
129. Dare, E.V., et al., *Fibrin sealants from fresh or fresh frozen plasma as scaffolds for in vitro articular cartilage regeneration.* Tissue Eng Part A, 2009. **15**(8): p. 2285-97.
130. Xu, J.-W., et al., *Injectable Tissue-Engineered Cartilage with Different Chondrocyte Sources.* Plastic and Reconstructive Surgery, 2004. **113**(5): p. 1361-1371.
131. Ahmed, T.A., E.V. Dare, and M. Hincke, *Fibrin: a versatile scaffold for tissue engineering applications.* Tissue Eng Part B Rev, 2008. **14**(2): p. 199-215.
132. Park, H., et al., *Injectable chitosan hyaluronic acid hydrogels for cartilage tissue engineering.* Acta Biomater, 2013. **9**(1): p. 4779-86.
133. Tan, H., et al., *Injectable in situ forming biodegradable chitosan-hyaluronic acid based hydrogels for cartilage tissue engineering.* Biomaterials, 2009. **30**(13): p. 2499-506.
134. Holland, T.A., Y. Tabata, and A.G. Mikos, *In vitro release of transforming growth factor-β1 from gelatin microparticles encapsulated in biodegradable, injectable oligo(poly(ethylene glycol) fumarate) hydrogels.* Journal of Controlled Release, 2003. **91**(3): p. 299-313.
135. Park, H., et al., *Delivery of TGF-beta1 and chondrocytes via injectable, biodegradable hydrogels for cartilage tissue engineering applications.* Biomaterials, 2005. **26**(34): p. 7095-103.
136. Park, H., et al., *Injectable biodegradable hydrogel composites for rabbit marrow mesenchymal stem cell and growth factor delivery for cartilage tissue engineering.* Biomaterials, 2007. **28**(21): p. 3217-27.

137. Jin, R., et al., *Synthesis and characterization of hyaluronic acid-poly(ethylene glycol) hydrogels via Michael addition: An injectable biomaterial for cartilage repair.* Acta Biomater, 2010. **6**(6): p. 1968-77.
138. Elisseeff, J., et al., *Transdermal photopolymeriation of poly(ethylene oxide)-based injectable hydrogels for tissue-engineered cartilage.* Tissue-Engineered Cartilage, 1999. **104**(4): p. 1014-22.
139. Werkmeister, J.A., et al., *Biodegradable and injectable cure-on-demand polyurethane scaffolds for regeneration of articular cartilage.* Acta Biomater, 2010. **6**(9): p. 3471-81.
140. Baraniak, P.R., et al., *Stiffening of human mesenchymal stem cell spheroid microenvironments induced by incorporation of gelatin microparticles.* J Mech Behav Biomed Mater, 2012. **11**: p. 63-71.
141. Solorio, L.D., et al., *Chondrogenic differentiation of human mesenchymal stem cell aggregates via controlled release of TGF-beta1 from incorporated polymer microspheres.* J Biomed Mater Res A, 2010. **92**(3): p. 1139-44.
142. Ravindran, S., et al., *Changes of chondrocyte expression profiles in human MSC aggregates in the presence of PEG microspheres and TGF-beta3.* Biomaterials, 2011. **32**(33): p. 8436-45.
143. Fan, H., et al., *Gelatin microspheres containing TGF-beta3 enhance the chondrogenesis of mesenchymal stem cells in modified pellet culture.* Biomacromolecules, 2008. **9**: p. 927-34.
144. Steinmetz, N.J. and S.J. Bryant, *Chondroitin sulfate and dynamic loading alter chondrogenesis of human MSCs in PEG hydrogels.* Biotechnol Bioeng, 2012. **109**(10): p. 2671-82.
145. Chen, W.C., et al., *Compare the effects of chondrogenesis by culture of human mesenchymal stem cells with various type of the chondroitin sulfate C.* J Biosci Bioeng, 2011. **111**(2): p. 226-31.
146. Lim, J.J., et al., *Development of nano- and microscale chondroitin sulfate particles for controlled growth factor delivery.* Acta Biomater, 2011. **7**(3): p. 986-95.
147. Bratt-Leal, A.M., et al., *Magnetic manipulation and spatial patterning of multi-cellular stem cell aggregates.* Integr Biol (Camb), 2011. **3**(12): p. 1224-32.
148. Box, G.E.P. and D.R. Cox, *An analysis of transformations.* Journal of the Royal Statistical Society Series B-Statistical Methodology, 1964. **26**(2): p. 211-252.
149. Ramakers, C., et al., *Assumption-free analysis of quantitative real-time polymerase chain reaction (PCR) data.* Neuroscience Letters, 2003. **339**(1): p. 62-66.
150. Glowacki, J., E. Trepman, and J. Folkman, *Cell Shape and Phenotypic Expression in Chondrocytes.* Experimental Biology and Medicine, 1983. **172**(1): p. 93-98.
151. Benya, P.D., S.R. Padilla, and M.E. Nimni, *Independent regulation of collagen types by chondrocytes during the loss of differentiated function in culture.* Cell, 1978. **15**: p. 1313-21.
152. Mayne, R., et al., *Changes in type of collagen synthesized as clones of chick chondrocytes grow and eveventually lose division capacity.* Proc Natl Acad Sci U S A, 1976. **73**: p. 1674-78.

153. Stokes, D.G., et al., *Assessment of the gene expression profile of differentiated and dedifferentiated human fetal chondrocytes by microarray analysis.* Arthritis Rheum, 2002. **46**(2): p. 404-19.
154. Zaucke, F., et al., *Cartilage oligomeric matrix protein (COMP) and collagen IX are sensitive markers for the differentiation state of articular primary chondrocytes.* Biochemical Journal, 2001. **358**: p. 17-24.
155. Kinner, B., J.M. Zaleskas, and M. Spector, *Regulation of Smooth Muscle Actin Expression and Contraction in Adult Human Mesenchymal Stem Cells.* Experimental Cell Research, 2002. **278**(1): p. 72-83.
156. Arora, P.D., N. Narani, and C.A.G. McCulloch, *The Compliance of Collagen Gels Regulates Transforming Growth Factor-β Induction of α-Smooth Muscle Actin in Fibroblasts.* The American Journal of Pathology, 1999. **154**(3): p. 871-882.
157. Willis, C.M. and M. Kluppel, *Inhibition by chondroitin sulfate E can specify functional Wnt/beta-catenin signaling thresholds in NIH3T3 fibroblasts.* J Biol Chem, 2012. **287**(44): p. 37042-56.
158. Khan, W.S., et al., *Bone marrow-derived mesenchymal stem cells express the pericyte marker 3G5 in culture and show enhanced chondrogenesis in hypoxic conditions.* J Orthop Res, 2010. **28**(6): p. 834-40.
159. Lim, J.J. and J.S. Temenoff, *The effect of desulfation of chondroitin sulfate on interactions with positively charged growth factors and upregulation of cartilaginous markers in encapsulated MSCs.* Biomaterials, 2013. **34**(21): p. 5007-18.
160. Carpenedo, R.L., S.A. Seaman, and T.C. McDevitt, *Microsphere size effects on embryoid body incorporation and embryonic stem cell differentiation.* J Biomed Mater Res A, 2010. **94**(2): p. 466-75.
161. Wang, Q.G., A.J. El Haj, and N.J. Kuiper, *Glycosaminoglycans in the pericellular matrix of chondrons and chondrocytes.* J Anat, 2008. **213**(3): p. 266-73.
162. Andrews, S.N., et al., *Optimization of microdermabrasion for controlled removal of stratum corneum.* Int J Pharm, 2011. **407**(1-2): p. 95-104.
163. Xie, L., et al., *Nondestructive assessment of sGAG content and distribution in normal and degraded rat articular cartilage via EPIC-microCT.* Osteoarthritis Cartilage, 2010. **18**(1): p. 65-72.